SWSC

RESEARCH ARTICLE

OPEN ⨕ ACCESS

The first *SEPServer* event catalogue ~68-MeV solar proton events observed at 1 AU in 1996–2010

Rami Vainio[1,*], Eino Valtonen[2], Bernd Heber[3], Olga E. Malandraki[4], Athanasios Papaioannou[4], Karl-Ludwig Klein[5], Alexander Afanasiev[1], Neus Agueda[6], Henry Aurass[7], Markus Battarbee[2], Stephan Braune[7], Wolfgang Dröge[8], Urs Ganse[8], Clarisse Hamadache[9], Daniel Heynderickx[10], Kalle Huttunen-Heikinmaa[2], Jürgen Kiener[9], Patrick Kilian[8], Andreas Kopp[3], Athanasios Kouloumvakos[11], Sami Maisala[1], Alexander Mishev[12], Rositsa Miteva[5], Alexander Nindos[11], Tero Oittinen[1], Osku Raukunen[2], Esa Riihonen[2], Rosa Rodríguez-Gasén[5,9], Oskari Saloniemi[2], Blai Sanahuja[6], Renate Scherer[3], Felix Spanier[8], Vincent Tatischeff[9], Kostas Tziotziou[4], Ilya G. Usoskin[12], and Nicole Vilmer[5]

[1] Department of Physics, University of Helsinki, 00014 Helsinki, Finland
*Corresponding author: e-mail: rami.vainio@helsinki.fi
[2] Department of Physics and Astronomy, University of Turku, 20014 Finland
[3] Institut für Experimentelle und Angewandte Physik, Christian-Albrechts-Universität zu Kiel, 24118 Kiel, Germany
[4] Institute of Astronomy, Astrophysics, Space Applications and Remote Sensing, National Observatory of Athens, 11810 Athens, Greece
[5] CNRS-LESIA, Observatoire de Paris, Meudon, France
[6] Dept. d'Astronomia i Meteorologia & Institut de Ciències del Cosmos, Universitat de Barcelona, Spain
[7] Solar Physics Group, Leibniz Institut für Astrophysik Potsdam, Germany
[8] Lehrstuhl für Astronomie, Julius-Maximilians Universität, Würzburg, Germany
[9] CSNSM Orsay, CNRS-IN2P3 et Université Paris-Sud, 91400 Orsay, France
[10] DH Consultancy BVBA, Leuven, Belgium
[11] Department of Physics, Section of Astrogeophysics, University of Ioannina, Greece
[12] Sodankylä Geophysical Observatory, Oulu Unit, University of Oulu, Finland

Received 20 June 2012 / Accepted 13 February 2013

ABSTRACT

SEPServer is a three-year collaborative project funded by the seventh framework programme (FP7-SPACE) of the European Union. The objective of the project is to provide access to state-of-the-art observations and analysis tools for the scientific community on solar energetic particle (SEP) events and related electromagnetic (EM) emissions. The project will eventually lead to better understanding of the particle acceleration and transport processes at the Sun and in the inner heliosphere. These processes lead to SEP events that form one of the key elements of space weather. In this paper we present the first results from the systematic analysis work performed on the following datasets: *SOHO*/ERNE, *SOHO*/EPHIN, *ACE*/EPAM, *Wind*/WAVES and *GOES* X-rays. A catalogue of SEP events at 1 AU, with complete coverage over solar cycle 23, based on high-energy (~68-MeV) protons from *SOHO*/ERNE and electron recordings of the events by *SOHO*/EPHIN and *ACE*/EPAM are presented. A total of 115 energetic particle events have been identified and analysed using velocity dispersion analysis (VDA) for protons and time-shifting analysis (TSA) for electrons and protons in order to infer the SEP release times at the Sun. EM observations during the times of the SEP event onset have been gathered and compared to the release time estimates of particles. Data from those events that occurred during the European day-time, i.e., those that also have observations from ground-based observatories included in *SEPServer*, are listed and a preliminary analysis of their associations is presented. We find that VDA results for protons can be a useful tool for the analysis of proton release times, but if the derived proton path length is out of a range of 1 AU $< s \lesssim 3$ AU, the result of the analysis may be compromised, as indicated by the anti-correlation of the derived path length and release time delay from the associated X-ray flare. The average path length derived from VDA is about 1.9 times the nominal length of the spiral magnetic field line. This implies that the path length of first-arriving MeV to deka-MeV protons is affected by interplanetary scattering. TSA of near-relativistic electrons results in a release time that shows significant scatter with respect to the EM emissions but with a trend of being delayed more with increasing distance between the flare and the nominal footpoint of the Earth-connected field line.

Key words. SEP – radiation – flares – radio emissions (dynamic) – projects

1. Introduction

Solar energetic particle (SEP) events are one of the most important elements of space weather (Vainio et al. 2009), being the defining component of solar radiation storms,[1] contributing to radio blackouts in polar regions and being related to many of the fastest coronal mass ejections (CMEs) driving major geomagnetic storms. In addition to CMEs, SEP events are also related to solar flares (e.g., Reames 1999). The occurrence rate of large, space-weather relevant SEP events is about 100 per solar cycle, with a broad distribution in time that extends well into the declining phase of the activity cycle as traced by the sunspot index.

Data Services and Analysis Tools for Solar Energetic Particle Events and Related Electromagnetic Emissions[2] (*SEPServer*) is a three-year collaborative project funded under the seventh framework programme (FP7-SPACE) of the European Union. The project started in December 2010. It will construct an Internet server that will provide access to a large number of SEP datasets from different instruments on-board half-a-dozen missions, to electromagnetic (EM) observations related to the events indentified from the SEP data, and to state-of-the art analysis tools that can be used to infer the solar SEP emission time profiles and interplanetary transport conditions prevailing during the SEP events. All datasets will be accompanied by comprehensive metadata as well as assessments of data quality. To assess their validity, the developed data-analysis methods will be compared against each other and solar EM observations. Furthermore, the project will provide analysis results on the events in the form of comprehensive SEP event catalogues that list key properties of the events. The server will be released to the community near the end of the project, in the fall of 2013.

This paper presents the SEPServer project and the results from the first year: the first SEP event catalogue. A systematic scan of the space-weather relevant[3] proton intensities (55–80 MeV, or ~68 MeV) observed by *SOHO*/ERNE was performed over the years 1996–2010. A total of 115 proton events were identified and analysed using data from *SOHO*/ERNE, *SOHO*/EPHIN and *ACE*/EPAM. We will present and discuss here the results of the analysis of these events. We concentrate on the onset analysis utilizing two different methods, velocity dispersion analysis (VDA) and time-shifting analysis (TSA), to get estimates of the particle release times close to the Sun. Furthermore, we analyse the EM associations of 44 of the events, i.e., those that occur during the day time in Europe and have the best coverage in terms of data available at *SEPServer*. The analysis is not meant to be comprehensive

but spawn a number of further efforts by the community, utilizing the data and preliminary analysis results presented in this paper. Likewise, while we attempt to compile a comprehensive list of events for the years 1996–2010, the resulting catalogue is not complete due to several data gaps and since the methodology applied misses some of the events that occur in the aftermath of another. Nevertheless, the community is encouraged to perform further studies making use of the *SEPServer* event catalogue for which full access will be provided through the project website (http://server.sepserver.eu).

The structure of the paper is the following. We present the *SEPServer* and the data it provides in detail in Section 2, describe the first SEP event catalogue produced by the project in Section 3, present and discuss the statistical analysis performed on the events in Section 4, and give our conclusions and outlook in Section 5.

2. The *SEPServer* project

The *SEPServer* project aims at facilitating access to a number of complementary SEP datasets, allowing in-depth analyses of SEP events to be performed. The emphasis of the project is on the space-weather relevant SEP events, i.e., events with proton spectra that extend to high enough energies to penetrate moderate shielding provided by spacecraft and constitute a space-weather hazard. The SEP datasets included in the project span over solar cycles 21–24 and the observations cover radial distances 0.3–5.4 AU. The SEP datasets distributed through *SEPServer* are listed in Table 1.

In addition to SEP data, crucial ingredients in the analysis of SEP events are the solar EM observations that are related to the events. Besides from context observations of, e.g., solar-wind plasma and magnetic field and CMEs related to the SEP event, important knowledge of the acceleration processes close to the Sun can be obtained from solar X-ray and gamma-ray observations as well as from solar radio observations that are generated by the accelerated particles, mostly electrons, that interact with the solar atmosphere. This occurs in the chromosphere and low corona for hard X-rays (HXR) and gamma-rays, and between the low corona and interplanetary space for radio-emitting electrons. While the CME observations are relatively easily accessible through a number of sources (e.g. *SOHO LASCO CME Catalog*[4], see Gopalswamy et al. 2009, and the automated *CACTUS* CME-detection facility[5], see Robbrecht et al. 2009), energetic photon and radio observations relevant to SEP events have not so far been collected to a single access point. Table 2 presents the EM observations distributed through *SEPServer*. At present, these datasets provide a comprehensive coverage of the identified high-energy proton events of the 23rd solar cycle. In future, they will be extended back to cover key events at earlier times, in particular the Nançay radioheliograph (available as 1-D imaging data for 1980–1995) and *AIP*/OSRA (to be recovered from microfilm archives) radio observations from the *Helios* era. These OSRA data have not been available in digital format prior to *SEPServer*. In addition to SEP and EM observations, *SEPServer* will provide local magnetic field data from each spacecraft of Table 1 carrying a magnetometer and plasma data from near-Earth solar wind (*ACE* and *Wind*).

---

[1] Here we adopt the terminology of NOAA, which provides scales for three types of space-sweather events (http://www.swpc.noaa.gov/NOAAscales/): solar radiation storms, radio blackouts and geomagnetic storms. The scale for solar radiation storms is based on the >10 MeV proton intensity observed by *GOES* spacecraft, the scale for radio blackouts on the soft-X-ray (SXR) flux observed by *GOES*, and the scale for the geomagnetic storms on the Kp index.

[2] http://www.sepserver.eu

[3] In this paper, we refer to as space weather relevant to those SEP events that extend to energies exceeding 55 MeV. The reasoning behind this selection is to concentrate on those events that are exceedingly difficult to shield against: geomagnetic shielding at the corresponding magnetic rigidity (320 MeV) at 1000 km altitude is ineffective at latitudes higher than 70° and the thickness of an Al shield stopping these protons has to exceed 1.28 cm (0.50″).

---

[4] http://cdaw.gsfc.nasa.gov/CME_list/

[5] http://sidc.oma.be/cactus/

Table 1. SEP datasets distributed through *SEPServer*.

Instrument	Time period covered	Distance (AU)	Species: energy range	Directional information
Helios-1&2/E6 Kunow et al. (1975)	01/1974–02/1986 (H1) 01/1976–/1980 (H2)	0.31–0.98 (H1) 0.29–0.98 (H2)	e^-: 0.3–>3.0 MeV p: 1.3–>51 MeV He: 1.7–48 MeV/n	55° view cone; two S/C; Sectorized ⊥ S/C-spin axis
Ulysses/HI-SCALE Lanzerotti et al. (1992)	01/1991–12/2006	1.3–5.4	e^-: 0.038–0.32 MeV ions: 0.061–4.8 MeV	Sectorized in various directions wrt. S/C-spin axis
Ulysses/COSPIN/KET Simpson et al. (1992)	01/1991–12/2006	1.3–5.4	e^-: 4–>500 MeV p: 2.7–>2000 MeV He: 2.3–>2100 MeV/n	45° view cone Sectorized ⊥ S/C-spin axis
Ulysses/COSPIN/LET Simpson et al. (1992)	01/1991–12/2006	1.3–5.4	p: 0.9–19 MeV He: 1–19 MeV/n CNO: 2.6–39 MeV/n $Z \geq 10$: 3.0–75 MeV/n	Sectorized ⊥ S/C-spin axis
Wind/3DP Lin et al. (1995)	11/1994–present	~1.0	e^-: 0.022–0.63 MeV p: 0.049–9.3 MeV	Eight true pitch-angle sectors Rebinned from 4π observations
SOHO/ERNE Torsti et al. (1995)	05/1996–present	~1.0	p: 1.6–130 MeV He: 1.6–130 MeV/n O: 2.5–200 MeV/n Fe-Ni: 3.0–200 MeV/n	62° and 120° view cones 250 bins within 120° view cone (3-axis stabilized S/C)
SOHO/EPHIN Müller-Mellin et al. (1995)	12/1995–present	~1.0	e^-: 0.25–10 MeV p: 4.3– MeV He: 4.3–53 MeV/n	Binned inside a 83° view cone (3-axis stabilized S/C)
ACE/SIS Stone et al. (1998)	08/1997–present	~1.0	He: 3.4–41 MeV/n O: 7.3–90 MeV/n Fe: 11–170 MeV/n	Integrated inside a 95° view cone (spinning S/C)
ACE/EPAM Gold et al. (1998)	08/1997–present	~1.0	e^-: 0.038–0.32 MeV ions: 0.047–4.8 MeV	Sectorized in various directions wrt. S/C-spin axis
STEREO-A&B/SEPT Müeller-Mellin et al. (2008)	11/2006–present	0.94–0.98 (A) 1.00–1.08 (B)	e^-: 0.065–0.43 MeV ions: 0.084–6.5 MeV	52° and 52.8° view cones; four directions; two 3-axis stabilized S/C
STEREO-A&B/LET Mewaldt et al. (2008)	11/2006–present	0.94–0.98 (A) 1.00–1.08 (B)	p: 1.8–15 MeV He: 4–15 MeV/n	Two 133° × 29° view cones; Two 3-axis stabilized S/C

In addition to a large number of well-documented datasets, *SEPServer* will provide the scientific community with state-of-the-art analysis tools based on numerical simulations of particle transport in the interplanetary medium. These tools allow one to deconvolve the effects of interplanetary transport from the observations in order to assess the source function of particle injection close to the Sun. This, in turn, can be directly compared with EM observations to perform accurate comparisons of the temporal and spectral relation between the interacting and escaping particles. The inversion tools (Agueda et al. 2008, 2009, 2012) are presently available for electron observations of *ACE*/EPAM, *Ulysses*/HI-SCALE and *Wind*/3DP. Work to implement the inversion methods for proton observations of the same instruments as well as on relativistic proton observations by the world network of neutron monitors is in progress. Note that certain criteria for the quality of observations (in terms of angular coverage and resolution and magnitude of the event) and quietness of the interplanetary medium have to be fulfilled in order for the simulation-based methods to be applicable (see Agueda et al. 2009). Thus, not all events distributed through *SEPServer* can be analysed using these methods.

The project will also perform scientific analysis of the SEP events using various kinds of data-analysis methods to investigate the relationship of the highest-energy proton and electron events and the corresponding EM solar observations. The methods employed range from the direct comparison of SEP and EM observations, applying TSA methods to crudely eliminate interplanetary particle transport effects, to the application of the simulation-based inversion methods. Direct data-analysis (DDA) methods[6] will be compared to the advanced inversion methods and to EM observations to assess the range of validity of the direct methods. For first results demonstrating the concept and capabilities of the approach, see Malandraki et al. (2012), who analysed the SEP event of 13 July 2005 in detail using the DDA and inversion methods, which will be distributed through *SEPServer*.

---

[6] The DDA methods refer to tools that can be used without resorting to simulation modelling. Such analyses include the event onset-time determination for SEP fluxes, e.g., for *SOHO*/EPHIN, *ACE*/EPAM and *SOHO*/ERNE in this study. This involves statistical methods like marking the onset at the time that the relevant flux exceeds the background level by 3σ or 4σ (used here for EPAM and EPHIN, respectively); alternatively, the Poisson-CUSUM method (Huttunen-Heikinmaa et al. 2005) (used here for ERNE; see p. 9) can be used. The derived onset times are then used to deduce solar release times using either TSA or VDA method.

Table 2. EM datasets distributed through *SEPServer*. Radio fluxes will be provided in solar flux units and HXR data in counting rates. The time resolution indicated is the one available through *SEPServer*.

Instrument	Type of instrument	Time period	Energy/ frequency	Spectral resolution	Time resolution
AIP/OSRA Mann et al. (1992)	Radio spectrograph	09/1994–07/2007	40–800 MHz	~0.7 MHz	1 s
ARTEMIS Kontogeorgos et al. (2006)	Radio spectrograph	01/1998–present	20–650 MHz	~1 MHz	1 s
Nançay/DA Lecacheux (2000)	Radio spectrograph	10/1991–present	20–70 MHz	0.1 MHz	~1.5 s
Wind/WAVES Bougeret et al. (1995)	Radio spectrograph	11/1994–present	0.02–1 MHz 1–14 MHz	4 kHz 50 kHz	1 min 1 min
Nançay/RH Kerdraon & Delouis (1997)	Radio heliograph	07/1996–present	150–450 MHz	Selected frequencies	10 s/32 s
INTEGRAL/SPI Vedrenne et al. (2003)	X- and γ-ray spectrometer	10/2002–present	0.02–8 MeV > 80 keV (ACS)	2.2 keV @ 1.33 MeV none (ACS)	1 s⁻¹ min 1 s
RHESSI Lin et al. (2002)	X- and γ-ray spectrometer	02/2002–present	3 keV–17 MeV	≤1 keV @ 3 keV, 5 keV @ >5 MeV	4 s

3. *SEPServer* proton event catalogue for the 23rd solar cycle

3.1. Event selection

In order to establish a catalogue of high-energy SEP events, which are particularly relevant for investigation of in-orbit space-weather effects, we visually scanned through *SOHO*/ERNE (Torsti et al. 1995) data for the time period from May 1996 till the end of 2010 extending over a full solar cycle. Intensity enhancements of protons in the energy range 54.8–80.3 MeV (average energy 67.7 MeV) were searched for.[7] The energy channel was purposely chosen well above the typically-used >10 MeV proton channel (e.g., Laurenza et al. 2009) available from *GOES* satellites. This was considered appropriate for the goals of the *SEPServer* project from the point of view of space-weather relevance, as discussed in the Introduction. Using this relatively high-energy range for event selection also allows more reliable identification of individual events in cases when events follow each other in rapid succession. In such cases small events at low energies tend to be masked by previous bigger events, while at high energies they can be better distinguished due to more rapid fall of intensities.

The selection criterion for the events in the *SEPServer* catalogue was that the 1 min average intensity in the 54.8–80.3 MeV ERNE proton channel was enhanced by a factor of ~3 above the quiet-time background of the appropriate phase of the solar cycle. During the observation period the quiet-time background varied from ~5 × 10⁻⁴ cm⁻² s⁻¹ sr⁻¹ MeV⁻¹ in 1996–1997 to ~3 × 10⁻⁴ cm⁻² s⁻¹ sr⁻¹ MeV⁻¹ in 2001–2003 and up to ~7 × 10⁻⁴ cm⁻² s⁻¹ sr⁻¹ MeV⁻¹ in 2009–2010. The total number of observed SEP events was 115 (Table 3). It should be noted that there were long breaks in the observations of the instrument from 25 June 1998 to 9 October 1998 and from 21 December 1998 to 8 February 1999 and several shorter data gaps as indicated in Table 3. The ERNE High Energy Detector

has a very large geometric factor (~20–40 cm² sr) often causing saturation during very large SEP events. Therefore, events following very large ones before the recovery of the instrument may have been missed. Such cases are, among others, the events of 17 and 20 January 2005 (Cane et al. 2010) following the event of 15 January 2005.

3.2. Solar release time determination

We carried out VDA for all 115 events using data with 1 min time resolution. The analysis was based on 20 proton energy channels between 1.58 MeV and 131 MeV (Table 4). *SOHO*/ERNE covers this energy range by using two different sensors. The Low-Energy Detector (LED) operates in the range 1.58 MeV to 13.8 MeV and the High-Energy Detector (HED) from 12.7 MeV to 131 MeV. Both sensors provide 10 energy channels. The geometric factor of LED is only about 1 cm² sr and thus the statistics in many events are relatively low at the highest-energy channels of LED. The geometric factor of HED is 20–40 cm² sr, depending on energy, making it possible to observe many events up to 100 MeV and above.

VDA of an SEP event is based on determining the onset times of the event at a number of energies and presenting these onset times as a function of the inverse velocity of the particles at respective energies. The velocity dispersion equation at 1 AU can be written as

$$t_{\mathrm{onset}}(E) = t_0 + 8.33 \, \frac{\min}{\mathrm{AU}} \, \mathrm{s} \, \beta^{-1}(E), \qquad (1)$$

where $t_{\mathrm{onset}}(E)$ is the observed onset time in minutes at proton kinetic energy E, t_0 is the release time (min) from the acceleration site, s is the apparent path length (AU) travelled by the particles and $\beta^{-1}(E) = \frac{c}{v(E)}$ is the inverse speed of the particles. Thus, by linear fitting of the onset times as a function of the corresponding inverse speed, an estimate for both the release time and the apparent path length of the particles can be obtained. Onset-time determination was done by using the so-called Poisson-CUSUM method (Huttunen-Heikinmaa et al. 2005). This is analogous to a statistical quality control scheme deciding whether or not a process is in control, and if not, giving the exact moment of time when the failure

---

[7] Due to different energy binning of *SOHO*/ERNE data before April 19, 2000, the energy range 54.4–79.2 MeV (average energy 67.5 MeV) was used before this date.

Table 3. Results of the *SOHO*/ERNE VDA for all 115 SEP events identified in the scan of observations in 1996–2010. X-ray flare information is obtained from Cane et al. (2010) (except for event E114, where the identification was ours; flare longitude was taken from Kanzelhöhe Observatory report). Items marked as "no flare" were all listed as events originating from far behind the west limb by Cane et al. (2010). (Note: pfu = cm^{-2} s^{-1} sr^{-1} MeV^{-1}; all times UT.)

	ERNE/55–80 MeV Proton Flux			X-ray flare			ERNE/Proton VDA			
ID	Date	Time	I_{max} (pfu)	Start	Class	ϕ [°]	$t_0 + 500$ s	s (AU)	R^2	Channels discarded
	ERNE data gaps: 28–31.05.1996; 02–03.06.1996; 25.02–04.03.1997									
E0	24.09.1997	03:59	1.5×10^{-3}	02:43	M6	19E	01:07 ± 26	5.63 ± 0.31	0.876	1–4
E1	07.10.1997	14:43	8×10^{-4}		No flare		12:55 ± 10	2.39 ± 0.13	0.951	19–20
	ERNE data gap: 25–28.10.1997									
E2	04.11.1997	06:41	1.5×10^{-1}	05:52	X2	33W	05:35 ± 07	2.44 ± 0.09	0.977	
E3	06.11.1997	12:37	1.5×10^{-1}	11:49	X9	63W	11:18 ± 06	3.94 ± 0.08	0.986	1–4
E4	13.11.1997	22:26	2×10^{-3}		No flare		21:40 ± 06	1.86 ± 0.06	0.854	1–3
E5	14.11.1997	14:29	1×10^{-3}		No flare		13:23 ± 14	2.19 ± 0.18	0.891	19–20
	ERNE data gaps: 19–21.11.1997; 25–28.02.1998									
E6	20.04.1998	11:13	1×10^{-1}	09:38	M1	90W	10:09 ± 10	2.55 ± 0.13	0.958	
E7	02.05.1998	14:10	1×10^{-1}	13:31	X1	15W	13:47 ± 08	1.16 ± 0.11	0.868	
E8	06.05.1998	08:29	4×10^{-1}	07:58	X3	65W	07:44 ± 14	1.39 ± 0.19	0.765	
E9	09.05.1998	04:32	6×10^{-3}	03:04	M8	100W	03:24 ± 10	2.56 ± 0.13	0.960	20
E10	16.06.1998	20:35	1×10^{-3}	18:03	M1	115W	19:21 ± 15	1.43 ± 0.19	0.762	19–20
	ERNE data gaps: 19–21.11.1997; 25–28.02.1998									
E6	20.04.1998	11:13	1×10^{-1}	09:38	M1	90W	10:09 ± 10	2.55 ± 0.13	0.958	
E7	02.05.1998	14:10	1×10^{-1}	13:31	X1	15W	13:47 ± 08	1.16 ± 0.11	0.868	
E8	06.05.1998	08:29	4×10^{-1}	07:58	X3	65W	07:44 ± 14	1.39 ± 0.19	0.765	
E9	09.05.1998	04:32	6×10^{-3}	03:04	M8	100W	03:24 ± 10	2.56 ± 0.13	0.960	20
E10	16.06.1998	20:35	1×10^{-3}	18:03	M1	115W	19:21 ± 15	1.43 ± 0.19	0.762	19–20
	ERNE data gaps: 24.06.–09.10.1998									
E11	18.10.1998	22:22	4×10^{-3}		No flare		No reasonable VDA result was found.			
E12	14.11.1998	06:16	1.5×10^{-1}		No flare		05:27 ± 05	1.23 ± 0.05	0.714	1–10
E13	22.11.1998	07:17	8×10^{-3}	06:30	X4	82W	06:43 ± 06	1.51 ± 0.09	0.952	
E14	24.11.1998	02:53	6×10^{-3}	02:07	X1	108W	02:14 ± 35	3.72 ± 0.46	0.781	20
	ERNE data gaps: 01–03.12.1998; 21.12.1998–08.02.1999; 14–18.02.1999									
E15	24.04.1999	14:30	3×10^{-3}		No flare		13:40 ± 07	1.75 ± 0.10	0.953	
E16	09.05.1999	18:40	2×10^{-3}	17:53	M8	95W	17:30 ± 08	2.35 ± 0.11	0.965	20
	ERNE data gap: 21–26.05.1999									
E17	27.05.1999	11:16	1×10^{-2}		No flare		10:30 ± 06	1.63 ± 0.08	0.964	20
E18	01.06.1999	19:49	1.8×10^{-2}		No flare		19:03 ± 11	2.26 ± 0.14	0.924	20
	ERNE data gap: 03–04.06.1999									
E19	11.06.1999	01:09	5×10^{-3}		No flare		00:32 ± 07	1.81 ± 0.09	0.963	
	ERNE data gaps: 19–20.8.1999; 15–20.11.1999; 07–08.01.2000									
E20	09.01.2000	21:30	8×10^{-4}		No flare		02:32 ± 22	4.55 ± 0.26	0.941	16–20
E21	18.01.2000	18:24	3×10^{-3}	17:07	M4	11E	No reasonable VDA result was found.			
E22	12.02.2000	05:15	1×10^{-3}	03:51	M1	24W	03:53 ± 11	2.91 ± 0.15	0.957	20
E23	17.02.2000	21:18	2×10^{-3}	20:17	M1	07E	20:49 ± 05	1.41 ± 0.06	0.951	1–2, 20
E24	18.02.2000	09:57	1.5×10^{-2}		No flare		09:59 ± 06	0.56 ± 0.09	0.721	
	ERNE data gap: 22–25.02.2000									
E25	02.03.2000	09:13	1.5×10^{-3}	08:20	X1	52W	08:08 ± 07	2.36 ± 0.09	0.977	20
E26	03.03.2000	02:47	1×10^{-3}	02:08	M4	60W	02:04 ± 06	1.91 ± 0.08	0.970	20
	ERNE data gap: 13–31.03.2000									
E27	04.04.2000	16:03	2×10^{-3}	15:12	C9	66W	15:20 ± 03	1.39 ± 0.04	0.987	19–20
E28	23.04.2000	14:00	2×10^{-3}		No flare		12:39 ± 20	3.46 ± 0.24	0.823	1–4, 20
	ERNE data gap: 22–24.05.2000									
E29	06.06.2000	18:25	4×10^{-3}	14:58	X2	14E	18:28 ± 07	0.79 ± 0.08	0.875	9–10, 14–15, 18, 20
E30	10.06.2000	17:26	2×10^{-1}	16:40	M5	40W	16:52 ± 04	1.56 ± 0.06	0.981	
E31	18.06.2000	02:29	1×10^{-3}	01:52	X1	85W	02:07 ± 10	1.06 ± 0.10	0.383	1–9, 20
E32	14.07.2000	10:37	$>1 \times 10^{-1}$	10:03	X6	07W	10:31 ± 09	1.05 ± 0.10	0.725	1–5, 11–12
E33	22.07.2000	12:03	1.5×10^{-2}	11:17	M4	56W	11:21 ± 04	2.23 ± 0.05	0.991	
E34	27.07.2000	23:06	2×10^{-3}		No flare		18:19 ± 76	8.26 ± 0.52	0.253	1–12, 18–20
E35	12.09.2000	13:09	1.5×10^{-2}	11:31	M1	09W	12:29 ± 09	1.76 ± 0.12	0.926	
E36	16.10.2000	07:39	2×10^{-3}	06:40	M2	95W	06:58 ± 05	1.52 ± 0.07	0.966	
E37	25.10.2000	12:40	2×10^{-3}	08:45	C4	120W	11:05 ± 26	1.79 ± 0.36	0.583	
E38	08.11.2000	23:20	$>6 \times 10^{-2}$	22:42	M7	75W	23:10 ± 01	0.46 ± 0.01	0.995	1–10, 12, 14, 20
E39	24.11.2000	05:43	7×10^{-2}	04:55	X2	03W	05:21 ± 14	2.02 ± 0.19	0.864	
E40	05.01.2001	18:33	2×10^{-3}		No flare		17:36 ± 10	2.20 ± 0.13	0.938	2, 19–20
E41	21.01.2001	04:40	2×10^{-3}		$t_{SEP} - t_X > 4$ h		08:30 ± 59	2.61 ± 0.80	0.372	19
E42	28.01.2001	16:58	5×10^{-2}	15:40	M2	59W	15:13 ± 17	3.89 ± 0.21	0.910	1–3
E43	29.03.2001	11:49	1.8×10^{-2}	09:57	X2	12W	10:20 ± 25	2.77 ± 0.35	0.786	
E44	02.04.2001	12:24	6×10^{-3}	10:58	X1	62W	12:39 ± 27	0.53 ± 0.38	0.103	
E45	02.04.2001	22:41	2×10^{-1}	21:32	X20	78W	22:31 ± 04	0.30 ± 0.04	0.791	1–2, 8–15
E46	09.04.2001	16:20	1.8×10^{-2}	15:20	M8	04W	No reasonable VDA result was found.			
E47	10.04.2001	07:34	4×10^{-2}	05:06	X2	09W	06:48 ± 11	1.38 ± 0.15	0.841	20
E48	12.04.2001	11:01	8×10^{-2}	09:39	X2	42W	10:35 ± 27	2.62 ± 0.37	0.740	

Table 3. Continued.

	ERNE/55–80 MeV Proton Flux			X-ray flare			ERNE/Proton VDA			
ID	Date	Time	I_{max} (pfu)	Start	Class	ϕ [°]	$t_0 + 500$ s	s (AU)	R^2	Channels discarded
E49	15.04.2001	14:05	1.5×10^{-1}	13:19	X14	84W	13:45 ± 07	1.57 ± 0.10	0.938	
E50	18.04.2001	02:51	2×10^{-1}	02:12	C2	120W	02:09 ± 05	1.95 ± 0.07	0.983	
E51	07.05.2001	13:05	6×10^{-3}		No flare		12:39 ± 07	1.44 ± 0.09	0.944	20
E52	20.05.2001	06:49	3×10^{-2}	06:00	M6	91W	05:48 ± 08	2.19 ± 0.11	0.962	
E53	04.06.2001	17:13	2×10^{-3}	16:11	C3	60W	16:20 ± 05	1.73 ± 0.06	0.982	19–20
E54	15.06.2001	16:08	4×10^{-2}		No flare		15:10 ± 06	2.32 ± 0.08	0.980	
E55	19.06.2001	04:17	8×10^{-3}		$t_{SEP} - t_X > 4$ h		03:20 ± 07	2.25 ± 0.09	0.943	1–4
ERNE data gap: 28–29.07.2001										
E56	10.08.2001	07:22	6×10^{-4}		Not listed		No reasonable VDA result was found.			
ERNE data gap: 10–17.08.2001										
E57	15.09.2001	12:24	3×10^{-3}	11:04	M2	53W	11:46 ± 05	1.32 ± 0.07	0.958	20
E58	24.09.2001	11:18	1×10^{-1}	09:32	X3	23E	10:26 ± 12	2.10 ± 0.16	0.892	1
E59	01.10.2001	08:53	2×10^{-2}		$t_{SEP} - t_X > 4$ h		11:52 ± 15	0.38 ± 0.19	0.177	18–20
E60	19.10.2001	01:58	7×10^{-3}	00:47	X2	18W	00:33 ± 23	3.30 ± 0.32	0.858	
E61	19.10.2001	17:22	1×10^{-2}	16:13	X2	29W	16:09 ± 12	3.08 ± 0.16	0.954	
E62	22.10.2001	15:51	2×10^{-2}	14:27	M7	18E	15:15 ± 08	1.66 ± 0.11	0.932	
E63	04.11.2001	16:45	$>1 \times 10^{-1}$	16:03	X1	18W	16:08 ± 09	1.45 ± 0.13	0.883	
E64	22.11.2001	20:54	5×10^{-2}	20:18	M4	67W	20:02 ± 06	2.49 ± 0.07	0.959	1–5
E65	26.12.2001	05:48	4×10^{-1}	04:32	M7	54W	04:43 ± 08	1.54 ± 0.12	0.912	
E66	10.01.2002	10:30	1×10^{-3}		Not listed		04:52 ± 65	5.94 ± 0.87	0.721	19
E67	14.01.2002	08:03	2×10^{-3}	05:29	M4	100W	09:58 ± 81	1.56 ± 1.09	0.108	10
E68	27.01.2002	13:38	5×10^{-3}		No flare		12:48 ± 05	2.34 ± 0.07	0.988	
ERNE data gap: 05–12.02.2002										
E69	20.02.2002	05:58	1×10^{-2}	05:52	M5	72W	05:44 ± 06	1.62 ± 0.08	0.960	19–20
E70	18.03.2002	04:16	4×10^{-3}	02:16	M1	100W	03:13 ± 05	2.81 ± 0.05	0.915	1–11, 19–20
E71	17.04.2002	10:32	2×10^{-3}	07:46	M3	34W	09:17 ± 07	1.81 ± 0.09	0.954	1, 18–20
E72	21.04.2002	01:45	$>5 \times 10^{-1}$	00:43	X2	84W	00:39 ± 12	2.20 ± 0.16	0.904	1
E73	22.05.2002	06:46	2×10^{-3}	03:18	C5	53W	00:48 ± 17	2.82 ± 0.21	0.905	17–20
E74	07.07.2002	12:13	5×10^{-3}	11:15	M1	95W	11:26 ± 04	1.77 ± 0.05	0.989	19–20
E75	16.07.2002	10:31	7×10^{-3}		$t_{SEP}\ t_X > 4$ h		07:55 ± 11	0.56 ± 0.14	0.477	18–20
E76	14.08.2002	06:44	2×10^{-3}		$t_{SEP}\ t_X > 4$ h		02:01 ± 07	1.29 ± 0.08	0.936	18–20
E77	18.08.2002	22:10	2×10^{-3}	21:12	M2	19W	21:40 ± 04	1.36 ± 0.04	0.843	1–10, 20
E78	20.08.2002	08:46	6×10^{-3}	08:22	M3	38W	08:01 ± 04	1.98 ± 0.04	0.966	1–7, 20
E79	22.08.2002	02:30	5×10^{-2}	01:47	M5	62W	01:37 ± 11	2.25 ± 0.15	0.931	
E80	24.08.2002	01:35	5×10^{-1}	00:49	X3	81W	00:34 ± 06	2.77 ± 0.08	0.987	
E81	06.09.2002	04:01	2×10^{-3}		$t_{SEP} - t_X > 4$ h		00:2109	0.89 ± 0.10	0.788	1, 15–20
E82	09.11.2002	14:37	5×10^{-3}	13:08	M5	29W	12:24 ± 14	3.84 ± 0.18	0.963	19–20
E83	19.12.2002	22:21	2×10^{-3}	21:34	M3	09W	21:52 ± 10	1.31 ± 0.11	0.605	1–7
ERNE data gap: 28.02.–11.03.2003										
E84	23.04.2003	01:32	2×10^{-3}	00:45	M5	25W	00:35 ± 14	2.24 ± 0.19	0.893	20
E85	28.05.2003	01:54	4×10^{-3}	00:17	X4	20W	02:46 ± 19	1.36 ± 0.25	0.624	20
E86	31.05.2003	02:56	5×10^{-2}	02:13	M9	65W	01:54 ± 11	2.82 ± 0.16	0.950	
E87	26.10.2003	17:55	$>1 \times 10^{-1}$	17:03	X1	38W	16:55 ± 12	2.16 ± 0.17	0.906	
E88	28.10.2003	11:18	$>1 \times 10^{-1}$	09:51	X17	08E	10:24 ± 09	2.74 ± 0.12	0.963	1, 11
E89	02.11.2003	10:05	7×10^{-2}		No flare		09:22 ± 25	2.94 ± 0.25	0.818	1, 12–20
E90	02.11.2003	17:54	$>2 \times 10^{-1}$	17:03	X8	56W	16:29 ± 24	3.79 ± 0.42	0.867	1–6, 11–15
E91	20.11.2003	08:59	3×10^{-3}	07:35	X1	08W	07:17 ± 17	1.21 ± 0.22	0.626	18–20
ERNE data gap: 19–22.01.2004										
E92	11.04.2004	05:00	4×10^{-3}	03:54	M1	46W	03:46 ± 11	2.65 ± 0.14	0.952	20
ERNE data gaps: 22–29.04.2004; 22–25.06.2004										
E93	13.07.2004	01:34	$>1 \times 10^{-3}$	00:09	M7	59W	01:08 ± 14	1.43 ± 0.18	0.773	19–20
E94	22.07.2004	17:33	2×10^{-3}		$t_{SEP} - t_X > 4$ h		14:01 ± 41	1.43 ± 0.56	0.268	20
E95	25.07.2004	16:19	3×10^{-3}	14:19	M2	33W	15:11 ± 26	2.61 ± 0.35	0.758	
ERNE data gap: 06–12.08.2004										
E96	01.11.2004	06:15	1×10^{-1}		No flare		05:11 ± 10	2.43 ± 0.13	0.954	
E97	07.11.2004	16:54	$>2 \times 10^{-2}$	15:42	X2	17W	14:36 ± 12	4.70 ± 0.14	0.953	1–5
E98	09.11.2004	18:43	$>5 \times 10^{-3}$	16:59	M9	51W	16:00 ± 30	7.94 ± 0.27	0.746	1–10, 20
E99	10.11.2004	02:46	$>5 \times 10^{-2}$	01:59	X3	49W	04:26 ± 02:10	3.25 ± 1.66	0.198	11–13
E100	15.01.2005	06:59	7×10^{-3}	05:54	M9	06E	06:23 ± 05	1.43 ± 0.07	0.961	20
E101	15.01.2005	23:35	5×10^{-2}	22:24	X3	05W	20:00 ± 19	5.27 ± 0.15	0.948	1–3, 11–20
E102	13.05.2005	18:43	5×10^{-3}	16:13	M8	11E	17:10 ± 06	1.47 ± 0.07	0.958	17–20
E103	16.06.2005	20:35	1×10^{-1}	20:01	M4	85W	19:51 ± 04	1.97 ± 0.05	0.979	1–3
E104	13.07.2005	22:23	1.5×10^{-3}		$t_{SEP} - t_X > 4$ h		14:31 ± 15	2.84 ± 0.19	0.924	18–20
E105	14.07.2005	11:59	1×10^{-2}	10:16	X1	89W	04:17 ± 67	14.56 ± 0.68	0.816	1–7, 20
E106	17.07.2005	13:03	9×10^{-3}		No flare		06:34 ± 50	16.24 ± 0.46	0.865	1–9, 20

Table 3. Continued.

ID	ERNE/55–80 MeV Proton Flux			X-ray flare			ERNE/Proton VDA			
	Date	Time	I_{max} (pfu)	Start	Class	ϕ [°]	t_0 + 500 s	s (AU)	R^2	Channels discarded
ERNE data gap: 31.07.–03.08.2005										
E107	22.08.2005	02:27	1.8×10^{-3}	00:44	M3	48W	01:29 ± 09	1.62 ± 0.12	0.914	19–20
E108	22.08.2005	17:53	8×10^{-3}	16:46	M6	60W	18:22 ± 09	2.06 ± 0.09	0.892	1–5, 18–20
E109	29.08.2005	14:28	2×10^{-3}		No flare		11:24 ± 46	4.07 ± 0.45	0.354	1–8, 19–20
E110	01.09.2005	01:59	3×10^{-3}		No flare		01:07 ± 26	5.63 ± 0.31	0.876	1–4, 20
ERNE data gap: 07–08.09.2005										
E111	06.07.2006	09:37	3×10^{-3}	08:13	M3	32W	08:34 ± 08	2.38 ± 0.10	0.970	20
ERNE data gap: 26.11.–11.12.2006 (many shortgaps)										
E112	13.12.2006	02:59	2×10^{-1}	02:14	X3	23W	02:58 ± 30	2.93 ± 0.40	0.756	14
E113	14.12.2006	23:08	8×10^{-2}	21:07	X2	46W	22:05 ± 09	2.67 ± 0.06	0.498	1–16
ERNE data gaps: 27–29.01.2007; 29.07.–14.08.2009; 07–24.09.2009										
E114	14.08.2010	10:41	7×10^{-3}	(09:38)	(C5)	(54W)	10:05 ± 06	1.23 ± 0.08	0.933	20
ERNE data gap: 10–15.12.2010										

happened. In this case, the failure is an SEP event causing intensities to rise above the pre-determined background. The updated algorithm used in this work allows changing background, which is often necessary to take into account, e.g., SEP events preceding the one under investigation, when the background has not yet reached a constant quiet-time value. Other criteria used for event onset determination were as described in Huttunen-Heikinmaa et al. (2005).

The SEP events investigated and the results of VDA are given in Table 3. Column 1 gives the identification number of the event, column 2 the date and column 3 the onset time (of 54.8–80.3 MeV protons) of the event. The maximum intensity, I_{max}, in column 4 indicates the size of the event as observed in the energy range 54.8 to 80.3 MeV by ERNE. Events with maximum intensity $\leq 1.0 \times 10^{-3}$ cm^{-2} s^{-1} sr^{-1} MeV^{-1} in this energy range are very weak and generally might not be observed at higher energies by ERNE. Columns 5–7 give the properties of the associated soft-X-ray flare as deduced by Cane et al. (2010), who considered the >25 MeV proton events in 1997–2006. However, we have not included their data on flares that are separated more than 4 h from the start of the event.[8] Note also that several events marked as "no flare" are actually events, where the parent solar activity occurred behind the limb Cane et al. (2010). The results of the VDA are listed in Columns 8 and 9, i.e., the deduced release time, t_0, and the apparent path length, s, travelled by particles with their standard errors, respectively. Column 10 gives the coefficient of determination (i.e. the squared linear correlation coefficient of the fit) related to the reliability of the results and describing the portion of the total variance in the onset time that can be explained as a linear relationship between the inverse velocity and the onset time. In column 11 the channel numbers of the data points discarded from the VDA are listed. In most of the events one or more data points were discarded from the VDA. The main reasons for discarding points were either high background from a previous event so that no additional enhancement was observed at low energies or the fact that the event did not cause noticeable intensity enhancement at the highest energies. Among the 115 analysed events there were four for which no reasonable velocity dispersion relation could be found. Also, for some events, while producing a fit of acceptable quality, VDA gives a value of the path length that can hardly be regarded as physical (either below 1 AU or much greater than it). As one purpose of this paper is to evaluate the performance of VDA, we have kept those events in the sample.

For electrons, we determined the onset times of the 115 events as observed by *SOHO*/EPHIN (Müeller-Mellin et al. 1995) and *ACE*/EPAM (Gold et al. 1998) in three energy channels: 0.18–0.31 MeV (EPAM), 0.3–0.7-MeV (EPHIN) and 0.7–3-MeV (EPHIN). The algorithm determines the average intensity I and the standard deviation σ inside the specified time window and compares the data just ahead of this window with a threshold $I + n\sigma$, where n can be chosen by the user (3σ and 4σ are used for EPAM and EPHIN, respectively). The onset is defined as the time stamp of the first point above the threshold. As all these electron channels have mean speeds close to the speed of light ($0.73c$, $0.86c$ and $0.98c$, respectively), the data do not really allow for VDA to be performed. We determined the onset times of the electron channels for each event and then performed a back-shifting of the onset times to get the release times of the electrons at the Sun:

$$t_{rel}(E) = t_{onset}(E) - 8.33 \frac{\min}{AU} L \beta^{-1}(E). \quad (2)$$

Rather than using the apparent path length obtained for protons, which is often severely affected by interplanetary scattering (Lintunen & Vainio 2004; Sáiz et al. 2005), we used the nominal length of the Parker spiral L computed for the solar-wind speed u_{sw} observed during the event, i.e.,

$$L(u_{sw}) = z(r_{s/c}) - z(R_\odot) \quad (3)$$

$$z(r) = \frac{a}{2} \left[\ln \left(\frac{r}{a} + \sqrt{1 + \frac{r^2}{a^2}} \right) + \frac{r}{a} \sqrt{1 + \frac{r^2}{a^2}} \right], \quad (4)$$

where $z(r)$ is the distance along an Archimedean spiral from the centre of the Sun, $r_{s/c}$ is the radial distance of the spacecraft from the Sun (here approximated as the position of *ACE*), $R_\odot$ is the solar radius, $a = u_{sw}/\Omega_\odot$ and $2\pi\Omega_\odot^{-1} = 24.47$ d is the equatorial period of solar rotation. For the solar-wind speed, we used data from *ACE*/SWEPAM[9]

---

[8] Note that we have also performed our own association of SXR flares with particles for 44 of the events, see below.

[9] http://www.srl.caltech.edu/ACE/ASC/level2/lvl2DATA_SWE-PAM.html

Table 4. Energy channels used in the SOHO/ERNE velocity dispersion analysis.

	Channel	Energy range (MeV)	Average energy (MeV)	Inverse speed (c^{-1})
LED	1	1.58–1.78	1.68	16.7
	2	1.78–2.16	1.97	15.5
	3	2.16–2.66	2.41	14.0
	4	2.66–3.29	2.98	12.6
	5	3.29–4.10	3.70	11.3
	6	4.10–5.12	4.71	10.0
	7	5.12–6.42	5.72	9.10
	8	6.42–8.06	7.15	8.15
	9	8.06–10.1	9.09	7.24
	10	10.1–12.7	11.4	6.47
HED	11	13.8–16.9	15.4	5.59
	12	16.9–22.4	18.9	5.06
	13	20.8–28.0	23.3	4.57
	14	25.9–32.2	29.1	4.11
	15	32.2–40.5	36.4	3.69
	16	40.5–53.5	45.6	3.32
	17	50.8–67.3	57.4	2.99
	18	63.8–80.2	72.0	2.70
	19	80.2–101	90.5	2.44
	20	101–131	108	2.26

(McComas et al. 1998), when available, substituted by data from *Wind*/SWE[10] (Ogilvie et al. 1995) when SWEPAM data was unavailable. The release time thus obtained represents an estimate of the latest possible release of electrons from the Sun that is consistent with the determined onset time at 1 AU. For comparison, we also performed the same type of TSA for 55–80-MeV protons observed by ERNE.

The results of the TSA are presented in Table 5. The first column gives the event ID (as in Table 3). The second column gives the nominal length of the Parker-spiral field line, columns 3–5 give the onset times for ERNE 55–80 MeV protons (from column 3 of Table 3), columns 6–7 give those for EPAM (for five events, the 0.18–0.31 MeV electron channel was replaced by the 0.10–0.18 MeV channel) and columns 9–12 for EPHIN. Column 8 gives a qualitative description of the electron anisotropy as observed by EPAM.[11] This may give an indication of how much scattering is experienced by electrons during interplanetary transport, but the beaming of the angular distribution may also be reduced by local field fluctuations at time scales shorter than the time resolution of the particle flux data. One could nevertheless regard the events with beam-like anisotropy as those with the most reliable release time. Note that we have added 500 s, i.e., the light travel time per AU, to the release time of each channel to allow an easier comparison with EM observations at 1 AU.

---

[10] http://web.mit.edu/space/www/wind/wind_data.html
[11] There are seven different options for pitch-angle distributions (PADs): (1) beam: clear well-pronounced beam-like structure is present; (2) moderate: anisotropic features are present but do not constitute a beam-like structure; (3) isotropic: no anisotropic features are presented; (4) bad coverage: all sectors were very close to each other in pitch-angle and no PAD is obtained; (5) irregular: denotes that it is impossible to characterize the anisotropic nature of the event through the calculated PADs; (6) E' contaminated: denotes that E' channels are contaminated so PADs cannot be formed (but deflected electrons can still be used for determining the onset); and (7) no data: denotes unavailability of sectored data.

3.3. Electromagnetic observations

SEPServer will also provide a wealth of EM observations on SEP events. In Table 6, we give the results of a preliminary analysis of SXR and radio observations for those 44 events that occur during the European day-time, i.e., for the events that *SEPServer* will provide the most extensive EM data coverage including results also from the ground-based observatories. In this paper, we concentrate on deka- and hectometric emission, obtained from *Wind*/WAVES, but further data from ground-based observatories at metric wavelengths is provided at our website in the form of summary plots of electromagnetic emissions.

The three first columns of the table give the event ID, the date and the solar release time (SRT) of protons, as deduced by the ERNE VDA. The fourth column shows the time of the impulsive flare phase. It is defined as the time between the start and the maximum of the SXR burst observed in the 0.1–0.8 nm channel of *GOES*. The start was computed as the time when the flux exceeded the pre-event background plus three times the noise level. The maximum is the time of the measured maximum of the burst, irrespective of considerations of the noise.

The characteristic times of type III emission were evaluated near 1 MHz. While the early emission is usually a well-defined type III burst, later phases are often mixed with less well-identified spectral features, such as spectrally complex type III bursts, or with type II emission. We inspected the plots of the dynamic spectra and then decided up to which time the emission was type III. The duration of the type III burst (Column 5) is the time interval during which the emission is at 3-sigma level above the background. For future reference, the number of bursts is evaluated from the flux density time profiles and checked by visual inspection of the dynamic spectra. Sometimes plateaus are observed, which look like an unresolved type III burst. These are generally counted as a burst, but the number is therefore to some extent subjective.

Table 5. Results of the *SOHO*/ERNE, *SOHO*/EPHIN and *ACE*/EPAM onset-time analysis for all 115 SEP events identified in the scan of ERNE observations in 1996–2010. All times UT.

		ERNE, 55–80 MeV			EPAM, 0.18–0.31 MeV			EPHIN, t_{onset} (t_{rel} + 500 s)			
ID	L (AU)	Date	t_{onset}	(t_{rel} + 500 s)	t_{onset}	(t_{rel} + 500 s)	Anisotropy	0.3–0.7 MeV		0.7–3 MeV	
E0	1.16	24.09.1997	03:59	(03:41)	03:43	(03:38)	Irregular	3:12	(03:09)	3:14	(03:12)
E1	1.20	07.10.1997	14:43	(14:24)	13:45	(13:40)	Moderate	13:15	(13:11)	13:23	(13:21)
E2	1.19	04.11.1997	06:41	(06:22)	06:19	(06:14)	Beam	6:16	(06:12)	6:16	(06:14)
E3	1.19	06.11.1997	12:37	(12:18)	12:37	(12:32)	Moderate	12:23	(12:19)	12:23	(12:21)
E4	1.19	13.11.1997	22:26	(22:07)	21:42	(21:37)	Beam	21:39	(21:35)	21:47	(21:45)
E5	1.18	14.11.1997	14:29	(14:10)	13:59	(13:54)	Moderate	13:45	(13:41)	13:46	(13:44)
E6	1.17	20.04.1998	11:13	(10:54)	10:43	(10:38)	Moderate	10:30	(10:27)	10:33	(10:31)
E7	1.07	02.05.1998	14:10	(13:54)	13:46	(13:42)	Beam	13:47	(13:45)	13:47	(13:46)
E8	1.06	06.05.1998	08:29	(08:13)	08:09	(08:06)	Bad μ-coverage	8:05	(08:03)	8:05	(08:04)
E9	1.09	09.05.1998	04:32	(04:15)	04:18	(04:14)	Isotropic	4:18	(04:15)	4:20	(04:19)
E10	1.18	16.06.1998	20:35	(20:16)	19:40	(19:35)	Bad μ-coverage	18:59	(18:55)	19:03	(19:01)
E11	1.13	18.10.1998	22:22	(22:04)	22:06	(22:02)	Moderate	21:30	(21:27)	21:32	(21:30)
E12	1.16	14.11.1998	06:16	(05:58)	05:28	(05:23)	Moderate	5:36	(05:33)	5:47	(05:45)
E13	1.15	22.11.1998	07:17	(06:59)	07:12	(07:08)	Moderate	7:03	(07:00)	7:00	(06:58)
E14	1.09	24.11.1998	02:53	(02:36)	02:55	(02:51)	Isotropic	2:42	(02:39)	3:07	(03:06)
E15	1.15	24.04.1999	14:30	(14:12)	13:49	(13:45)	Moderate	13:38	(13:35)	13:47	(13:45)
E16	1.18	09.05.1999	18:40	(18:21)	18:20*	(18:15)*	Beam*	18:13	(18:09)	18:17	(18:15)
E17	1.14	27.05.1999	11:16	(10:58)	11:06	(11:02)	Beam	10:58	(10:55)	11:00	(10:58)
E18	1.22	01.06.1999	19:49	(19:29)	19:30	(19:25)	Bad μ-coverage	19:21	(19:17)	19:20	(19:17)
E19	1.15	11.06.1999	01:09	(00:51)	01:00	(00:56)	Beam	0:53	(00:50)	0:55	(00:53)
E20	1.21	09.01.2000	21:30	(21:10)		No event			Complex		
E21	1.21	18.01.2000	18:24	(18:04)	18:08	(18:03)	Irregular		Complex	17:59	(17:57)
E22	1.06	12.02.2000	05:15	(04:59)	04:48	(04:45)	E' contaminated	4:39	(04:37)	4:51	(04:50)
E23	1.14	17.02.2000	21:18	(21:00)	21:06	(21:02)	Beam	20:56	(20:53)	21:01	(20:59)
E24	1.14	18.02.2000	09:57	(09:39)	09:34	(09:30)	Beam	9:33	(09:30)	9:33	(09:31)
E25	1.13	02.03.2000	09:13	(08:55)	08:45	(08:41)	Beam	8:40	(08:37)	8:43	(08:41)
E26	1.15	03.03.2000	02:47	(02:29)	02:34	(02:30)	Bad μ-coverage	2:30	(02:27)	2:31	(02:29)
E27	1.18	04.04.2000	16:03	(15:44)	15:28	(15:23)	Beam	15:24	(15:20)	15:25	(15:23)
E28	1.18	23.04.2000	14:00	(13:41)	13:56	(13:51)	E' contaminated	13:21	(13:17)	13:32	(13:30)
E29	1.17	06.06.2000	18:25	(18:06)	18:20	(18:15)	E' contaminated	16:43	(16:40)	16:43	(16:41)
E30	1.13	10.06.2000	17:26	(17:08)	17:11	(17:07)	Beam	17:07	(17:04)	17:08	(17:06)
E31	1.18	18.06.2000	02:29	(02:10)	02:26	(02:21)	E' contaminated	02:13	(02:09)	02:15	(02:13)
E32	1.09	14.07.2000	10:37	(10:20)	10:39	(10:35)	Moderate	10:16	(10:13)	10:16	(10:15)
E33	1.17	22.07.2000	12:03	(11:44)	11:53	(11:48)	No data	11:50	(11:47)	11:55	(11:53)
E34	1.22	27.07.2000	23:06	(22:46)	00:20	(00:15)	E' contaminated	23:44	(23:40)	23:43	(23:40)
E35	1.19	12.09.2000	13:09	(12:50)	12:45	(12:40)	Beam	12:28	(12:24)	12:36	(12:34)
E36	1.08	16.10.2000	07:39	(07:22)	07:37	(07:33)	Beam	07:29	(07:26)	07:48	(07:47)
E37	1.15	25.10.2000	12:40	(12:22)	11:26	(11:22)	Moderate	10:54	(10:51)	11:02	(11:00)
E38	1.11	08.11.2000	23:20	(23:03)	23:01	(22:57)	Beam	22:58	(22:55)	22:58	(22:56)
E39	1.19	24.11.2000	05:43	(05:24)	05:47	(05:42)	Moderate	05:32	(05:28)	05:32	(05:30)
E40	1.13	05.01.2001	18:33	(18:15)	18:40	(18:36)	Irregular	17:36	(17:33)	17:44	(17:42)
E41	1.24	21.01.2001	04:40	(04:20)	04:23	(04:18)	Irregular	21:49	(21:45)	21:49	(21:46)
E42	1.22	28.01.2001	16:58	(16:38)	16:49	(16:44)	Moderate	16:25	(16:21)	16:28	(16:25)
E43	1.09	29.03.2001	11:49	(11:32)	10:31	(10:27)	Isotropic	10:23	(10:20)	10:23	(10:22)
E44	1.08	02.04.2001	12:24	(12:07)	12:14	(12:10)	Moderate		No data		
E45	1.09	02.04.2001	22:41	(22:24)	22:04	(22:00)	Beam		No data		
E46	1.08	09.04.2001	16:20	(16:03)	16:23	(16:19)	E' contaminated	16:17	(16:14)	16:11	(16:10)
E47	1.09	10.04.2001	07:34	(07:17)	07:32	(07:28)	E' contaminated	07:09	(07:06)	07:09	(07:08)
E48	1.06	12.04.2001	11:01	(10:45)		No event			Complex		
E49	1.11	15.04.2001	14:05	(13:48)	14:05	(14:01)	Moderate	14:02	(13:59)	14:02	(14:00)
E50	1.11	18.04.2001	02:51	(02:34)	02:47	(02:43)	Beam	02:35	(02:32)	02:35	(02:33)
E51	1.19	07.05.2001	13:05	(12:46)	12:37	(12:32)	Moderate	09:53	(09:49)	10:03	(10:01)
E52	1.18	20.05.2001	06:49	(06:30)	06:44	(06:39)	Moderate	06:26	(06:22)	06:30	(06:28)
E53	1.16	04.06.2001	17:13	(16:55)	16:51	(16:46)	Bad μ-coverage	16:46	(16:43)	16:50	(16:48)
E54	1.27	15.05.2001	16:08	(15:47)	15:57	(15:51)	Beam	15:54	(15:50)	15:53	(15:50)
E55	1.15	19.06.2001	04:17	(03:59)	03:55	(03:51)	Beam	03:49	(03:46)	03:48	(03:46)
E56	1.16	10.08.2001	07:22	(07:04)		No event		15:54	(15:51)	15:54	(15:52)
E57	1.08	15.09.2001	12:24	(12:07)	12:05*	(12:01)*	Moderate*	11:53	(11:50)	12:08	(12:07)
E58	1.13	24.09.2001	11:18	(11:00)	10:55	(10:51)	Beam	10:52	(10:49)	10:52	(10:50)
E59	1.10	01.10.2001	08:53	(08:36)	13:11	(13:07)	Isotropic		Complex		
E60	1.28	19.10.2001	01:58	(01:37)	01:55	(01:49)	Moderate	01:49	(01:44)	01:49	(01:46)
E61	1.21	19.10.2001	17:22	(17:02)	17:19	(17:14)	Beam	17:05	(17:01)	17:12	(17:10)
E62	1.09	22.10.2001	15:51	(15:34)	15:41	(15:37)	E' contaminated	15:32	(15:29)	15:33	(15:32)
E63	1.22	04.11.2001	16:45	(16:25)	16:43	(16:38)	Beam	16:31	(16:27)	16:33	(16:30)
E64	1.11	22.11.2001	20:54	(20:37)	20:56	(20:52)	Contaminated	20:49	(20:46)	20:52	(20:50)
E65	1.16	26.12.2001	05:48	(05:30)	05:35	(05:30)	Moderate	22:29	(22:26)	22:33	(22:31)

*The 0.10–0.18 MeV energy channel used instead.

Table 5. Continued.

ID	L (AU)	ERNE, 55–80 MeV			EPAM, 0.18–0.31 MeV			EPHIN, t_{onset} (t_{rel} + 500 s)			
		Date	t_{onset}	(t_{rel} + 500 s)	t_{onset}	(t_{rel} + 500 s)	Anisotropy	0.3–0.7 MeV		0.7–3 MeV	
E66	1.10	10.01.2002	10:30	(10:13)	10:32	(10:28)	Isotropic	09:13	(09:10)	09:18	(09:16)
E67	1.08	14.01.2002	08:03	(07:46)	No event			09:21	(09:18)	09:20	(09:19)
E68	1.18	27.01.2002	13:38	(13:19)	12:58*	(12:53)*	Beam*	12:58	(12:54)	13:21	(13:19)
E69	1.14	20.02.2002	05:58	(05:40)	06:05	(06:01)	Beam	06:02	(05:59)	06:02	(06:00)
E70	1.30	18.03.2002	04:16	(03:54)	04:54	(04:48)	E' contaminated	12:11	(12:06)	12:11	(12:08)
E71	1.13	17.04.2002	10:32	(10:14)	10:27	(10:23)	Isotropic	08:36	(08:33)	08:45	(08:43)
E72	1.13	21.04.2002	01:45	(01:27)	01:37	(01:33)	Beam	01:32	(01:29)	01:34	(01:32)
E73	1.19	22.05.2002	06:46	(06:27)	00:31*	(00:26)	Beam*	00:19	(00:15)	00:19	(00:17)
E74	1.17	07.07.2002	12:13	(11:54)	12:03	(11:58)	Beam	11:47	(11:44)	11:48	(11:46)
E75	1.23	16.07.2002	10:31	(10:11)	08:06	(08:01)	Irregular	00:57	(00:53)	04:43	(04:40)
E76	1.15	14.08.2002	06:44	(06:26)	01:59	(01:55)	Beam	01:56	(01:53)	01:57	(01:55)
E77	1.09	18.08.2002	22:10	(21:53)	21:53	(21:49)	E' contaminated	21:31	(21:28)	21:36	(21:35)
E78	1.13	20.08.2002	08:46	(08:28)	08:42	(08:38)	Beam	08:32	(08:29)	08:31	(08:29)
E79	1.19	22.08.2002	02:30	(02:11)	02:23	(02:18)	Beam	02:07	(02:03)	02:15	(02:13)
E80	1.18	24.08.2002	01:35	(01:16)	01:26	(01:21)	Beam	01:01	(00:57)	01:02	(01:00)
E81	1.17	06.09.2002	04:01	(03:42)	03:00	(02:55)	Bad μ-coverage	00:00	(23:57)	00:00	(23:58)
E82	1.19	09.11.2002	14:37	(14:18)	14:06	(14:01)	Beam	13:42	(13:38)	13:49	(13:47)
E83	1.07	19.12.2002	22:21	(22:05)	22:01	(21:57)	Beam	21:57	(21:55)	21:58	(21:57)
E84	1.10	23.04.2003	01:32	(01:15)	01:21	(01:17)	Beam	01:17	(01:14)	01:21	(01:19)
E85	1.08	28.05.2003	01:54	(01:37)	01:07	(01:03)	Moderate	01:00	(00:57)	01:00	(00:59)
E86	1.05	31.05.2003	02:56	(02:40)	02:39	(02:36)	Beam	02:35	(02:33)	02:35	(02:34)
E87	1.11	26.10.2003	17:55	(17:38)	17:48	(17:44)	Beam	17:45	(17:42)	17:45	(17:43)
E88	1.03	28.10.2003	11:18	(11:03)	11:21*	(11:18)	Beam*	12:00	(11:58)	12:00	(11:59)
E89	1.07	02.11.2003	10:05	(09:49)	09:56	(09:52)	Moderate	10:01	(09:59)	10:01	(10:00)
E90	1.09	02.11.2003	17:54	(17:37)	17:36	(17:32)	Beam	17:15	(17:12)	17:15	(17:14)
E91	1.05	20.11.2003	08:59	(08:43)	07:28	(07:25)	E' contaminated	06:50	(06:48)	06:50	(06:49)
E92	1.14	11.04.2004	05:00	(04:42)	04:44	(04:40)	E' contaminated	04:33	(04:30)	04:43	(04:41)
E93	1.12	13.07.2004	01:34	(01:16)	01:13	(01:09)	No data	00:40	(00:37)	00:48	(00:46)
E94	1.10	22.07.2004	17:33	(17:16)	17:36	(17:32)	Moderate	09:46	(09:43)	09:54	(09:52)
E95	1.10	25.07.2004	16:19	(16:02)	15:29	(15:25)	Isotropic	15:21	(15:18)	15:21	(15:19)
E96	1.15	01.11.2004	06:15	(05:57)	06:09	(06:05)	Bad μ-coverage	06:04	(06:01)	06:04	(06:02)
E97	1.09	07.11.2004	16:54	(16:37)	16:47	(16:43)	E' contaminated	Complex			
E98	1.04	09.11.2004	18:43	(18:27)	17:40	(17:37)	E' contaminated	18:00	(17:58)	18:00	(17:59)
E99	1.03	10.11.2004	02:46	(02:31)	02:38	(02:35)	Moderate	Complex			
E100	1.04	15.01.2005	06:59	(06:43)	06:54	(06:51)	Moderate	06:37	(06:35)	06:46	(06:45)
E101	1.07	15.01.2005	23:35	(23:19)	23:32	(23:28)	Moderate	00:02	(00:00)	00:02	(00:01)
E102	1.10	13.05.2005	18:43	(18:26)	17:32	(17:28)	Isotropic	17:19	(17:16)	17:28	(17:26)
E103	1.07	16.06.2005	20:35	(20:19)	20:30	(20:26)	Moderate	20:25	(20:23)	20:25	(20:24)
E104	1.09	13.07.2005	22:23	(22:06)	14:33	(14:29)	Beam	14:27	(14:24)	14:36	(14:35)
E105	1.12	14.07.2005	11:59	(11:41)	09:19	(09:15)	Moderate	11:42	(11:39)	11:42	(11:40)
E106	1.16	17.07.2005	13:03	(12:45)	13:06	(13:01)	Isotropic	13:24	(13:21)	13:23	(13:21)
E107	1.12	22.08.2005	02:27	(02:09)	01:18	(01:14)	Beam	01:10	(01:07)	01:11	(01:09)
E108	1.11	22.08.2005	17:53	(17:36)	17:33	(17:29)	Moderate	17:23	(17:20)	17:27	(17:25)
E109	1.19	29.08.2005	14:28	(14:09)	12:42	(12:37)	Isotropic	11:50	(11:46)	12:02	(12:00)
E110	1.11	01.09.2005	01:59	(01:42)	01:39	(01:35)	No data	00:06	(00:03)	00:16	(00:14)
E111	1.09	06.07.2006	09:37	(09:20)	09:21	(09:17)	Moderate	09:05	(09:02)	09:25	(09:24)
E112	1.04	13.12.2006	02:59	(02:43)	02:47	(02:44)	Bad μ-coverage	02:26	(02:24)	02:29	(02:28)
E113	1.01	14.12.2006	23:08	(22:53)	22:41	(22:38)	E' contaminated	22:10	(22:08)	22:10	(22:09)
E114	1.16	14.08.2010	10:41	(10:23)	10:20	(10:15)	No data	10:11	(10:08)	10:18	(10:16)

4. Results and discussion

4.1. Analysis of VDA results

The analysed 115 SEP events provide some statistics for the derived apparent path lengths. The apparent path length distribution seems to be double-peaked (Fig. 1). The first maximum is at 1.4 AU, close to the nominal Parker spiral length. The second peak is at longer apparent path lengths at 2.2 AU. The statistics, however, are not very high with 14 events in the first and 11 events in the second maximum 0.2-AU wide bin. Thus, as evidenced by the 1σ statistical error limits in the histogram, the statistical significance of the second maximum is not very large. There are also several events for which either very long (>5 AU, 8 cases) or very short (<1 AU, 8 cases) apparent path lengths were found. With the exception of three cases, the linear VDA fit to the data in these events was poor. In two of the exceptional cases (08.11.2000 and 15.01.2005) only seven data points were accepted for the fit.

The apparent path length and the spiral length of the field line are compared in Figure 2. There is almost no correlation between the two quantities. The VDA path length is typically longer than the length of the spiral field line, as expected, and it seems that other factors, such as pre-event background

Table 6. Summary of electromagnetic observations of 44 SEP events identified in the scan of ERNE observations in 1996–2010, for which European day-time observations are available. All times UT.

ID	Date	SRT + 500 s	SXR Imp. phase	DH type III	
		(ERNE)	(GOES)	Duration	Number
E1	07.10.1997	12:55 ± 10	Occulted	12:51–12:59	1
E3	06.11.1997	11:18 ± 06	11:51–11:55	11:52–12:05	3
E5	14.11.1997	13:23 ± 14	Peak < 12 UT	13:00–13:13	3
E6	20.04.1998	10:09 ± 10	Occulted	10:03–10:33	5
E7	02.05.1998	13:47 ± 08	13:30–13:42	13:34–14:04	4
E8	06.05.1998	07:44 ± 14	08:00–08:10	07:59–08:24	4
E15	24.04.1999	13:40 ± 07	No SXR burst	13:10–13:22	1
E17	27.05.1999	10:30 ± 06	No SXR burst	10:38–11:13	5
			11:34–11:45	11:52–11:58	1
E24	18.02.2000	09:59 ± 06	09:21–09:28	09:18–09:34	3
E25	02.03.2000	08:08 ± 07	08:21–08:28	08:24–08:51	5
E27	04.04.2000	15:20 ± 03	15:03–15:42	15:17–15:43	3*
E28	23.04.2000	12:39 ± 20	Uncertain	12:22–13:24	7
E29	06.06.2000	18:28 ± 07	15:01–15:26	15:10–15:34	7
E32	14.07.2000	10:31 ± 09	10:06–10:25	10:12–11:04	13
E33	22.07.2000	11:21 ± 04	11:09–11:13	11:09–11:16	2
			11:16–11:34	11:30–11:47	5
E35	12.09.2000	12:29 ± 09	11:16–12:13	11:46–12:30	11
E36	16.10.2000	06:58 ± 05	06:41–07:40	06:52–07:40	4*
E37	25.10.2000	11:05 ± 26	08:52–11:26	10:01–10:25	3
E43	29.03.2001	10:20 ± 25	09:34–10:17	09:59–10:27	7
E44	02.04.2001	12:39 ± 27	10:55–11:36	11:00–11:19	3*
E47	10.04.2001	06:48 ± 11	04:43–05:26	05:10–05:50	10
				06:58–07:06	1
E48	12.04.2001	10:35 ± 27	10:07–10:30	10:18–10:52	6
E49	15.04.2001	13:45 ± 07	13:20–13:50	13:40–14:55	12
E51	07.05.2001	12:39 ± 07	11:17–12:20	11:54–11:59	1*
E54	15.05.2001	15:10 ± 06	No SXR burst	15:30–15:54	3
E57	15.09.2001	11:46 ± 05	11:03–11:28	11:33–12:04	3
E58	24.09.2001	10:26 ± 12	09:28–10:40	09:43–10:55	12
E62	22.10.2001	15:15 ± 08	14:13–15:09	15:02–15:35	7
E68	27.01.2002	12:48 ± 05	12:13–12:15	12:10–12:26	3
E71	17.04.2002	09:17 ± 07	07:40–08:24	07:55–08:45	7
E74	07.07.2002	11:26 ± 04	10:42–11:44	11:08–11:58	8
E75	16.07.2002	07:55 ± 11	Uncertain		Storm
E78	20.08.2002	08:01 ± 04	08:25–08:27	08:25–08:39	2
E82	09.11.2002	12:24 ± 14	13:06–13:24	13:08–14:16	11
E88	28.10.2003	10:24 ± 09	09:44–11:10	10:06–11:25	16
E89	02.11.2003	09:22 ± 25	Uncertain		
E91	20.11.2003	07:17 ± 17	07:26–07:47	07:30–08:12	7
E95	25.07.2004	15:11 ± 26	14:22–15:20	14:26–15:24	7
E100	15.01.2005	06:23 ± 05	05:37–06:42	06:07–06:15	2
E102	13.05.2005	17:10 ± 06	16:14–16:57	16:42–17:07	3
E104	13.07.2005	14:31 ± 15	13:54–14:50	14:03–14:29	4*
E106	17.07.2005	06:34 ± 50	06:15–06:30		Storm
E111	06.07.2006	08:34 ± 08	08:09–08:38	08:18–08:52	7
E114	14.08.2010	10:05 ± 06	09:23–10:05	09:55–10:18	3

*Indicates that DH type III bursts occur only during the impulsive phase of the flare.

variability and/or non-simultaneous release at different energies, contribute to the apparent path length much more than the actual length of the field line, although the trend line in the figure has a reasonable slope, i.e., somewhat exceeding unity. However, the statistical significance for the fit is very low so this could be entirely fortuitous.

Next, we investigated the relation between the proton release times obtained from TSA and VDA methods. Figure 3 gives the difference of the two release times as a function of the difference of the apparent VDA path length and the calculated spiral length, s-L. The slope of the trend line, 19.4 min AU^{-1}, is close to $v^{-1} = 23.1$ min AU^{-1} for 67.7 MeV protons, which indicates that the basic assumptions of the VDA analysis are not unreasonable. If one subtracts the trend line from the release time difference, the data points show a standard deviation of 38 min. Thus, there is quite significant scatter of the points around the trend line, which can be due to several contributing factors. First, the scatter reflects the inaccuracies in the determination of the onset time for some events as, for example, previous events can yield a high background masking the start of the
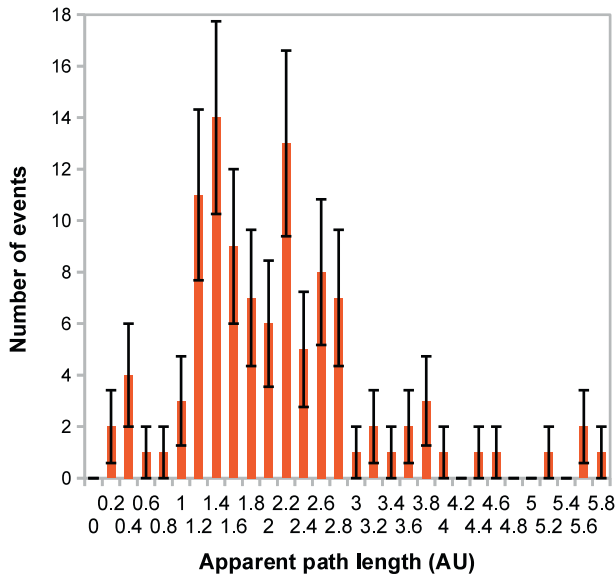
Fig. 1. Apparent path length distribution of 107 SEP events. Four events with apparent path lengths above 6 AU are not shown in the figure. The numbers on the abscissa denote the lower limit of the path length bin.
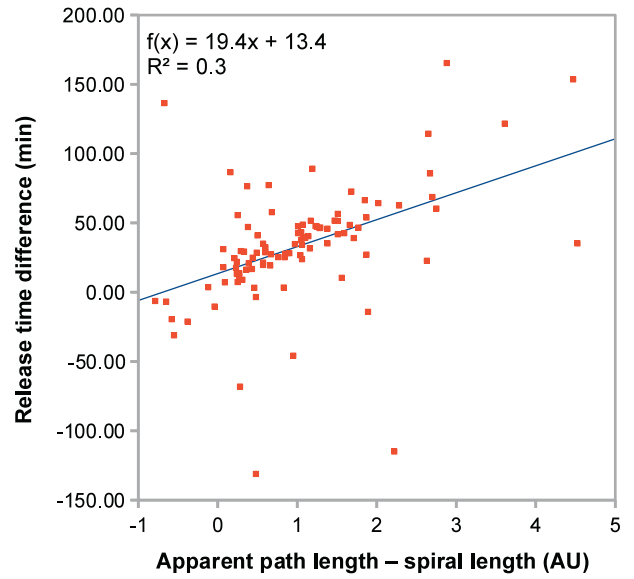

Fig. 3. The difference between the TSA (67.7 MeV, using the spiral length) and VDA (1.6–130 MeV) release times for protons as a function of the difference of VDA path length and the spiral length. Events with release time difference greater than 3 hours have been dropped from the analysis.
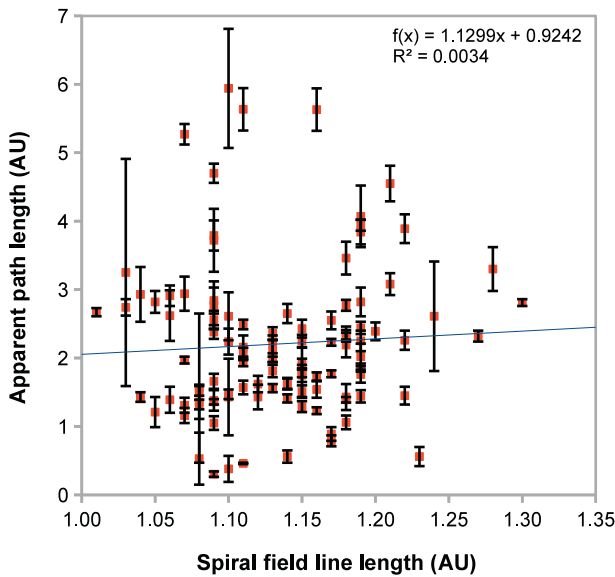
Fig. 2. The apparent path length obtained from VDA against the length of the Archimedean spiral field line. The error bars are obtained from the VDA.
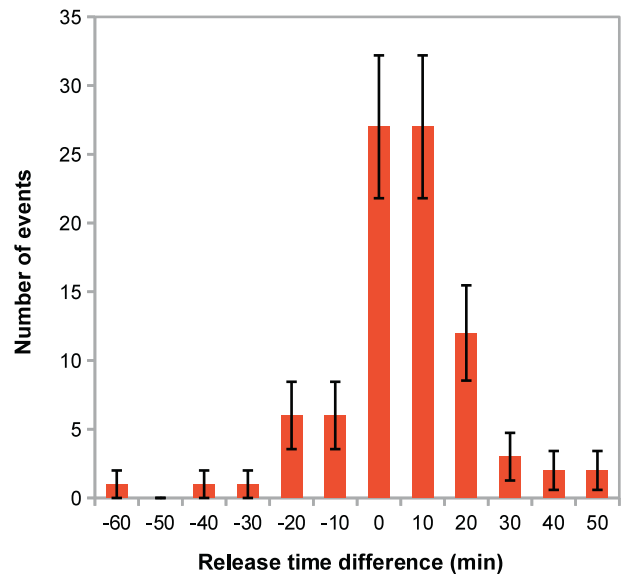
Fig. 4. The distribution of 67.7 MeV proton release time differences as obtained from TSA (using the VDA path length) and VDA, respectively. The value of the difference equals the difference between the actual 67.7 MeV onset time and the value obtained from the VDA fit at 67.7 MeV. Events with differences more than an hour have been dropped. The mean value and the standard deviation of the difference are 10 min and 17 min, respectively. The error bars denote the statistical error, only. The numbers on the abscissa denote the lower limit of the time difference bin.

event at some energy channels. Second, some of the scatter is probably also due to energy-dependent release times at the Sun.[12]

If one compares the VDA release time with the 67.7-MeV proton release time as obtained using TSA, but replacing the spiral field-line length L in Eq. (2) with s obtained from the VDA, one gets an estimate of the scatter that is due to the variation of the onset time in a particular channel with respect to

the trend line obtained in VDA. Figure 4 presents the distribution of the difference of the release times of 67.7-MeV protons obtained this way. The mean value and the standard deviation of the difference are 10 min and 17 min, respectively. Note that the value of the mean is close to the 13 min intercept obtained from the trendline in Figure 3. Thus, there is evidence that the

---

[12] Note that according to VDA of numerical simulation results (Lintunen & Vainio 2004) energy-dependent transport processes contribute relatively little to the accuracy of the VDA.
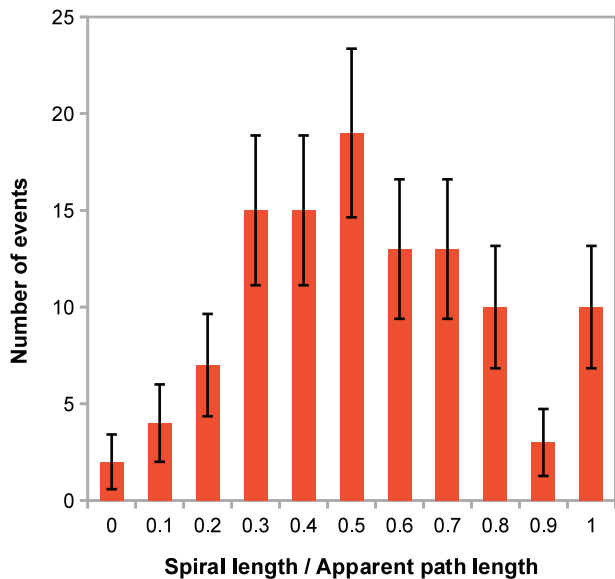
Fig. 5. The distribution of the ratio of the length of the Archimedean spiral field line to the apparent path length obtained from VDA. The quantity represents an estimate of the effective value of μ of the first-arriving particles. The total number of events is 111. The error bars denote the statistical error, only. The numbers on the abscissa denote the lower limit of the μ bin and the last bin is integral.

Fig. 6. The distribution of the difference of the apparent release times of *SOHO*/EPHIN 0.3–0.7 MeV and *ACE*/EPAM 0.18–0.31 MeV electrons. Twelve events with an onset-time difference of more than an hour were omitted. The error bars denote the statistical error, only. The numbers on the abscissa denote the lower limit of the time difference bin.

release of 67.7-MeV protons occurs somewhat later than the mean release time of particles included in the VDA.

One way of comparing the apparent path length to the spiral length of the field line is to analyse the statistics of their ratio. This is because we can write

$$ds = v\,dt = \frac{v\,dl}{v\mu} = \mu^{-1}dl, \qquad (5)$$

where dl is the length increment of the field line connecting the source and the observer and μ is pitch-angle cosine of the particles, so the obtained value of the apparent path length could be interpreted as

$$s = \overline{\mu^{-1}}\,l, \qquad (6)$$

where l is the actual length of the field line connecting the source and the observer and the overbar denotes an average value obtained for the first-arriving particles during their propagation from the source near the Sun to 1 AU. If one takes $l = L$, the ratio L/s gives an estimate of the effective value of μ as $\mu_{\rm eff} = 1/\overline{\mu^{-1}}$. Figure 5 presents the distribution of $\mu_{\rm eff} = L/s$ obtained from all the 111 events with a VDA result. Excluding the unphysical values (the integral bin), the mean value and standard deviation of $\mu_{\rm eff}$ are 0.54 and 0.21, respectively, which seem reasonable in light of simulation studies (Lintunen & Vainio 2004; Sáiz et al. 2005).

4.2. Analysis of solar release times and flare onset

Next, we studied the estimated release times (from TSA) of relativistic electrons. The difference of the release times in two energy channels is plotted in Figure 6. Although the scatter is significant, electrons at higher energies have earlier TSA release times than electrons at lower enegies. There is an average difference of 4.6 min between the estimated release time of 0.7–3 MeV and 0.3–0.7 MeV electrons, in this case so that

the higher energy electrons are released later. This could partly result from underestimation of the path length travelled by first-observed electrons, but since the delay of the lower energies is quite large, 9.0 min on average for events included in Figure 6, this explanation would require the true path length to exceed the spiral field-line lengths by more than 5 AU, which is unlikely. Moreover, instrumental effects cannot be ruled out as the two channels are measured by two different instruments.

Finally, we compared the particle release times with the start times of the related SXR flares as given by Cane et al. (2010). The delay of near-relativistic (NR; 0.18–0.3 MeV) electron emission with respect to X-ray emission is plotted as a function of the flare longitude $\phi_{\rm fl}$ in Figure 7a. The shortest delay is obtained in the region of well-connected flares, around 60–80° solar longitude. Figure 7b presents the same points as a function of longitudinal distance of the solar flare from the footpoint of the Parker spiral leading to Earth, as obtained from the solar-wind speed observed during the SEP event onset:

$$\Delta\phi = \left| \phi_{\rm fl} - \frac{\Omega_\odot r_{\rm S/C}}{u_{\rm sw}} \right|. \qquad (7)$$

Both pictures show a clear delay of the onset of events with poor magnetic connection to the flare. The linear fit to the data points in Figure 7b gives a slope of 0.34 min/degree, which would correspond to an azimuthal speed at the solar surface of 590 km s^{-1}, which is of the same order of magnitude with typical lateral speeds of CME-related disturbances in the corona (Warmuth & Mann 2011; Cheng et al. 2012). This possibly indicates that the evolution of the CME related to the event has a role in the release of the accelerated particles on field lines connected to the observer. Note, however, that the quality of our SRT determination, as evidenced by the large scatter of the individual points in Figures 7a and 7b, is not enough to reach a definitive conclusion on this issue. We note also that
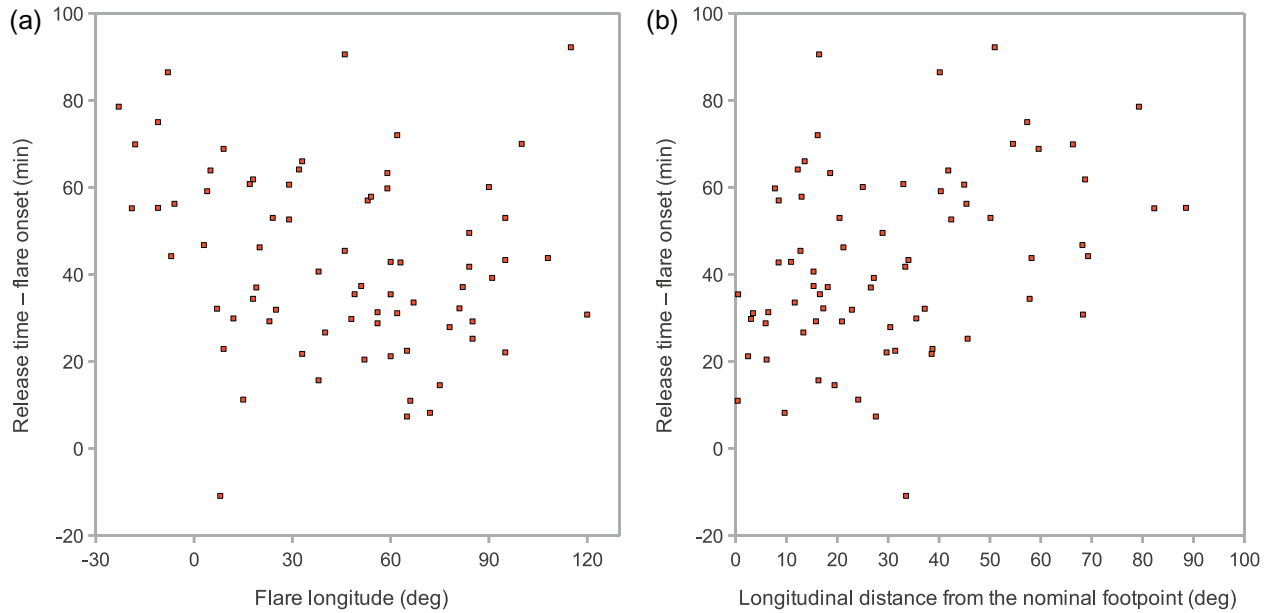
(a)

(b)

Fig. 7. The apparent SRT of NR electrons, as observed by *ACE*/EPAM, relative to the flare onset as a function of (a) the longitude of the parent flare; and (b) the longitudinal distance of the flare from the footpoint of the Archimedean spiral field.
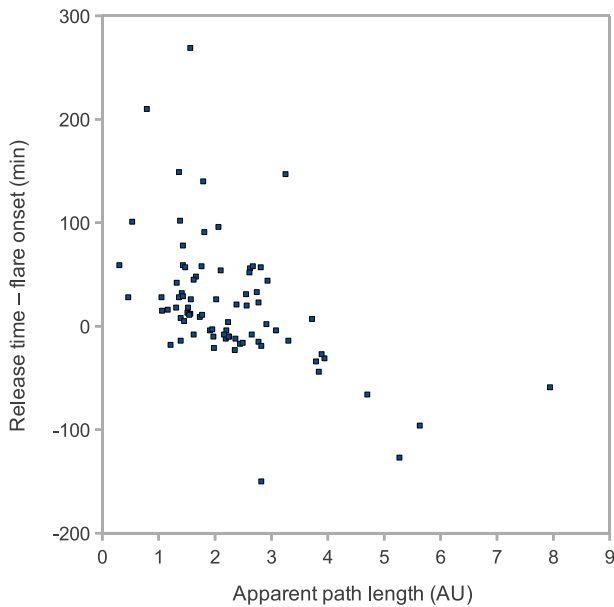

Fig. 8. The apparent SRT of protons (*SOHO*/ERNE VDA) with respect to the associated X-ray flare onset as a function of the apparent path length.

the onset-time determination for widely separated events might be compromised by lower early intensities in these events.

Figure 8 gives the release times of protons as obtained from VDA as a function of apparent path length. This figure indicates that nearly all events with $1 < s \lesssim 3$ AU have reasonable proton release times that are independent of the path length. However, at path length values outside this range there is a tendency of the release time to shift towards earlier values for larger values of the path length. This would be expected if the true path length in these events actually had a value inside the expected range. Thus, probably the apparent path length values outside

$1 < s \lesssim 3$ AU are artefacts of the analysis and the related release times should not be trusted. A similar result was obtained by Lintunen & Vainio (2004) analysing simulated data.

4.3. Associations with EM emissions

Next, we will turn to the timing of proton release with respect to the escape to space of energetic electrons at keV energies as traced by DH type III bursts. For a preliminary discussion we use the 44 events that occurred during the day time in Europe, listed in Table 6. We will compare the SRT of protons inferred from ERNE with the time of DH type III bursts observed by Wind/WAVES and the time of the impulsive flare phase inferred from GOES SXR observations. In Table 6 we only consider SXR and radio emission near the SRT inferred from the ERNE VDA. This explains why some of the identifications differ from those in the Cane et al. (2010) event list, which we used in Table 3.

The duration of the impulsive phase of the SXR emission (Column 4) is the interval between the time where the GOES time profile (0.1–0.8 nm wavelength) exceeded the background by 3σ and the time of maximum. Slight differences may exist with the start times listed in Table 3. Decametric-kilometric type III bursts were detected in all events, but sometimes they were embedded in type III storms, and an exact delimitation of the bursts related to the parent activity of the SEP event with respect to the storm bursts was difficult. Column 5 of Table 6 gives the time interval where the emission at 1 MHz was above the background + 3σ level. Event E75 (2002 July 16) occurred during a type III storm, but had no conspicuous DH type III burst near the SRT window. The brightest type III burst between the solar release time inferred from velocity dispersion analysis and the start of the event at ERNE occurred near 9 UT east of central meridian, as observed by the Nançay Radioheliograph. Because of its location it is not an obvious tracer of the release of the protons detected by ERNE. Event E89 was also classified as uncertain in Table 6, because no clear type III emission was observed at the high-frequency limit of the WAVES

spectrograph. But prominent type III and type II emission was seen at lower frequencies during the release time interval of the protons inferred from the velocity dispersion analysis.

In the other 42 events we found the following timing of the DH type III bursts with respect to the SRT of 68 MeV protons:

– In nine events (21%) the SRT interval inferred from VDA preceded the DH type III emission (E3, E8, E17, E25, E47, E54, E78, E82, E106) by between a few minutes (E17) and more than 4 h (E106).
– In nine other (21%) events (E15, E24, E29, E37, E44, E51, E68, E71, E100) the SRT interval lagged behind the end of the DH type III emission by between a few minutes (E100) and nearly 3 h (E29).
– In 24 events (57%) the SRT interval overlapped with an interval of intense DH type III burst emission.

The majority of the events (to which event E89 has to be added) hence show a time coincidence between the inferred window of initial proton release and the DH type III bursts, which signal electron beams travelling through the high corona into interplanetary space.

The differences found in other events indicate either a failure of the VDA or physical delays between the releases of deka-MeV protons and keV electrons (cf. Malandraki et al. 2012, for the 2005 July 13 event). Comparing the path lengths derived from VDA and the type III timing in the three event categories derived from the type III timing, we find the following:

– Extremely long path lengths inferred from VDA are found in events E3 ($s = 3.94$ AU), E82 ($s = 3.84$ AU) and E106 ($s = 16.34$ AU). In these three events the SRT preceded the DH type III groups by particularly long durations, ranging from 34 min to nearly 5 h (E106). In the other events where the SRT was inferred to occur before the type III bursts the delays varied between 8 and 24 minutes.
– Events with unphysically short path lengths ($s < 1$ AU; E24, E29, E44) are in the group where the SRT inferred from VDA lags behind the end of the DH type III bursts by between several tens of minutes and several hours. The events with the longest lags, about 3 h (E29) and 2.2 h (E44), had both unphysically short path lengths.
– Events where the solar release time inferred from VDA overlaps with the DH type III bursts have apparent path lengths between 1.05 and 3.46 AU.

This corroborates our conclusion that extreme path lengths inferred from VDA, above 3-4 AU as well as below 1 AU, are due to a failure of the method. The initial solar release of deka-MeV protons appears to be closely related in time to the DH type III bursts.

Next, we compare the timing of the radio and X-ray emission. Out of a total of 44 SEP events listed, nine had no clear SXR burst, probably because they occurred behind the solar limb. One event (E106) had no clear DH type III burst at the time of the inferred solar release of protons and the associated SXR burst. So 34 events allow for a clear association of SXR emission with DH type III bursts. The relative timing of the DH type III bursts with respect to the SXR burst is the following:

– In 6 events (18%) DH type III bursts occur only during the impulsive phase, i.e., during the rise phase of the SXR

profile (*GOES*, 0.1–0.8 nm). These events are labelled with an "asterisk" in Column 7 of Table 6.
– In 28 events (82%) the DH type III emission starts during the impulsive flare phase and extends beyond the peak of the SXR emission.
– In no case does the DH type III emission start after the SXR peak.

Thus, it seems that the electrons producing the type III burst have direct access to open field lines during the energy release of the flare. Note that these electrons are not necessarily the same as those observed in situ, so the result is not in contradiction with the delayed release of NR electrons of poorly connected events. However, an alternative interpretation would be that the delay is not real but due to the compromised timing of particle release in nominally poorly connected events, as discussed above.

5. Conclusions and outlook

We have performed a scan of 55–80 MeV proton fluxes observed by *SOHO*/ERNE in 1996–2010. A total of 115 SEP events were identified from this time period. We performed a VDA on all the proton events, using ERNE observations in 20 energy channels at 1.6–130 MeV, to get estimates of the SRT and path length in the interplanetary medium of the first-arriving protons. The results were compared to a TSA method utilizing the Archimedean spiral field-line length as the path length of first-arriving protons. In addition to protons, TSA was performed also to relativistic electrons observed by *ACE*/EPAM and *SOHO*/EPHIN.

A preliminary statistical analysis was performed on the VDA and TSA results, comparing them to each other and to the timing of the GOES X-ray flares related to the particle events, as identified by Cane et al. (2010). VDA was seen to produce reasonable results, in the sense that the two parameters, s and t_0 (relative to the flare onset), appeared independent of each other, provided that the apparent path length obtained from the analysis was in the range $1 < s \lesssim 3$ AU. Outside this range the parameters appeared to be anticorrelated. TSA compared to VDA produced the expected result that TSA release time (for 67.7 MeV protons) appeared later in most cases. This was true also if instead of the spiral length of the field line, the VDA path length was used to obtain the TSA release time.

Interpreting the higher-than-nominal values of the apparent path length of protons obtained from VDA as a signature of interplanetary scattering, we detemined the distribution $\mu_{\rm eff} = 1/\overline{\mu^{-1}}$ for first-observed particles. The events showed a distribution that had a maximum in the 0.5–0.6 bin, with a mean value calculated over the sample as $\mu_{\rm eff} = 0.54$. This indicates that the scattering mean free path in the interplanetary medium is typically well below 1 AU, since even the first-arriving protons propagate with path lengths about 1.9 times their nominal values.

TSA for 0.18–0.31 MeV electrons was performed to study the release time of electrons with respect to the onset of the SXR flare. The time delay of the electron release with respect to the X-rays was studied as a function of flare longitude. While there was significant scatter among the events, the trend of the delay was consistent with the longitudinal expansion of the electron emission region at the speed of about 600 km s^{-1}. This seems consistent with the typical lateral expansion speed of the erupting structures in the corona, but the result may also

be fortuitous, as the onset-time determination for widely separated events might be compromised. In fact, our result indicating the coincidence of initial proton release and DH Type III radio emission for events that conform to the expected range of VDA path lengths suggests that this might be the case.

The results of our preliminary analysis can be freely utilized in future studies. In addition to the tabulated information presented in this paper, our website (http://server.sepserver.eu) will offer access to summary plots of particle fluxes and EM observations related to the events. In addition to the catalogue of 1-AU observations made during the 23rd solar cycle, we will prepare catalogues of energetic particle events observed by the Helios and Ulysses missions and upgrade the 1-AU observations with particle events of the 24th solar cycle, including events observed by the twin-spacecraft *STEREO* mission (Kaiser et al. 2008).

References

Agueda, N., R. Vainio, D. Lario, and B. Sanahuja, Injection and interplanetary transport of near-relativistic electrons: modeling the impulsive event on 2000 May 1, *Astrophys. J.*, **675**, 1601–1613, 2008.

Agueda, N., R. Vainio, D. Lario, B. Sanahuja, E. Kilpua, and S. Pohjolainen, Modeling solar near-relativistic electron events. Insights into solar injection and interplanetary transport conditions, *A&A*, **507**, 981–993, 2009.

Agueda, N., R. Vainio, and B. Sanahuja, A database of >20 keV electron green's functions of interplanetary transport at 1 AU, *Astrophys. J. Suppl. Ser.*, **202**, 18, 2012.

Bougeret, J.-L., M.L. Kaiser, P.J. Kellogg, R. Manning, K. Goetz, et al., The radio and plasma wave investigation on the wind spacecraft, *Space Sci. Rev.*, **71**, 231–263, 1995.

Cane, H.V., I.G. Richardson, and T.T. von Rosenvinge, A study of solar energetic particle events of 1997–2006: their composition and associations, *J. Geophys. Res.*, **115**, A08101, 2010.

Cheng, X., J. Zhang, O. Olmedo, A. Vourlidas, M.D. Ding, and Y. Liu, Investigation of the formation and separation of an extreme-ultraviolet wave from the expansion of a coronal mass ejection, *Astrophys. J.*, **745**, L5, 2012.

Gold, R.E., S.M. Krimigis, S.E. HawkinsIII, D.K. Haggerty, D.A. Lohr, E. Fiore, T.P. Armstrong, G. Holland, and L.J. Lanzerotti, Electron, proton, and alpha monitor on the advanced composition explorer spacecraft, *Space Sci. Rev.*, **86**, 541–562, 1998.

Gopalswamy, N., S. Yashiro, G. Michalek, G. Stenborg, A. Vourlidas, S. Freeland, and R. Howard, The SOHO/LASCO CME catalog, *Earth, Moon and Planets*, **104**, 295–313, 2009.

Huttunen-Heikinmaa, K., E. Valtonen, and T. Laitinen, Proton and helium release times in SEP events observed with SOHO/ERNE, *A&A*, **442**, 673–685, 2005.

Kaiser, M.L., T.A. Kucera, J.M. Davila, O.C. St.Cyr, M. Guhathakurta, and E. Christian, The STEREO mission: an introduction, *Space Sci. Rev.*, **136**, 5–16, 2008.

Kerdraon, A., and J.-M. Delouis, The Nançay radioheliograph, in *Coronal physics from radio and space observations*, edited by G., Trottet, Springer Lecture Notes in Physics Series, **483**, 192–201, 1997.

Kontogeorgos, A., P. Tsitsipis, C. Caroubalos, X. Moussas, P. Preka-Papadema et al., The improved ARTEMIS IV multichannel solar radio spectrograph of the University of Athens, *Exp. Astron.*, **21**, 41–55, 2006.

Kunow, H., G. Wibberenz, G. Green, R. Müeller-Mellin, M. Witte, and H. Hempe, The Kiel University experiment for measuring cosmic radiation between 1.0 and 0.3 AU E 6, *Raumfahrtforschung*, **19**, 253–258, 1975.

Lanzerotti, L.J., R.E. Gold, K.A. Anderson, T.P. Armstrong, R.P. Lin, S.M. Krimigis, M. Pick, E.C. Roelof, E.T. Sarris, and G.M. Simnett, Heliosphere instrument for spectra, composition and anisotropy at low energies, *A&AS*, **92**, 349–363, 1992.

Laurenza, M., E.W. Cliver, J. Hewitt, M. Storini, A.G. Ling, C.C. Balch, and M.L. Kaiser, A technique for short-term warning of solar energetic particle events based on flare location, flare size, and evidence of particle escape, *Space Weather*, **7**, S04008, 2009.

Lecacheux, A., The Nançay Decameter Array: a useful step towards giant, new generation radio telescopes for long wavelength radio astronomy. in *Radio Astronomy at Long Wavelengths*, edited by R.G., Stone, K.W. Weiler, M.L. Goldstein, and J.-L. Bougeret, AGU Monograph Series, **119**, 321–328, 2000.

Lin, R.P., K.A. Anderson, S. Ashford, C. Carlson, D. Curtis, et al., A three-dimensional plasma and energetic particle investigation for the wind spacecraft, *Space Sci. Rev.*, **71**, 125–153, 1995.

Lin, R.P., B.R. Dennis, G.J. Hurford, D.M. Smith, A. Zehnder, et al., The Reuven Ramaty High-Energy Solar Spectroscopic Imager (RHESSI), *Sol. Phys.*, **210**, 3–32, 2002.

Lintunen, J., and R. Vainio, Solar energetic particle event onset as analyzed from simulated data, *A&A*, **420**, 343–350, 2004.

Malandraki, O., N. Agueda, A. Papaioannou, K.-L. Klein, E. Valtonen, et al., Scientific analysis within SEPServer – new perspectives in solar energetic particle research: the case study of the 13 July 2005 event, *Sol. Phys.*, **281**, 333–352, 2012.

Mann, G., H. Aurass, W. Voigt, and J. Paschke, Preliminary observations of solar type II bursts with the new radiospectrograph in Tremsdorf (Germany), *Coronal Streamers, Coronal Loops, and Coronal and Solar Wind Composition*, ESA SP, **348**, 129–132, 1992.

McComas, D.J., S.J. Bame, P. Barker, W.C. Feldman, J.L. Phillips, P. Riley, and J.W. Griffee, Solar Wind Electron Proton Alpha Monitor (SWEPAM) for the advanced composition explorer, *Space Sci. Rev.*, **86**, 563–612, 1998.

Mewaldt, R.A., C.M.S. Cohen, W.R. Cook, A.C. Cummings, A.J. Davis, et al., The Low-Energy Telescope (LET) and SEP central electronics for the STEREO mission, *Space Sci. Rev.*, **136**, 285–362, 2008.

Müller-Mellin, R., H. Kunow, V. Fleißner, E. Pehlke, E. Rode, et al., COSTEP – Comprehensive Suprathermal and Energetic Particle Analyser, *Sol. Phys.*, **162**, 483–504, 1995.

Müller-Mellin, R., S. Böttcher, J. Falenski, E. Rode, L. Duvet, T. Sanderson, B. Butler, B. Johlander, and H. Smit, The solar electron and proton telescope for the STEREO mission, *Space Sci. Rev.*, **136**, 363–389, 2008.

Ogilvie, K.W., D.J. Chornay, R.J. Fritzenreiter, F. Hunsaker, J. Keller, et al., SWE, A comprehensive plasma instrument for the wind spacecraft, *Space Sci. Rev.*, **71**, 55–77, 1995.

Reames, D.V., Particle acceleration at the Sun and in the heliosphere, *Space Sci. Rev.*, **90**, 413–491, 1999.

Robbrecht, E., D. Berghmans, and R.A.M. Van der Linden, Automated LASCO CME catalog for Solar cycle 23: Are CMEs scale invariant?, *Astrophys. J.*, **691**, 1222–1234, 2009.

Sáiz, A., P. Evenson, D. Ruffolo, and J.W. Bieber, On the estimation of solar energetic particle injection timing from onset times near Earth, *Astrophys. J.*, **626**, 1131–1137, 2005.

Simpson, J.A., J.D. Anglin, A. Balogh, M. Bercovitch, J.M. Bouman, et al., The ULYSSES cosmic ray and solar particle investigation, *A&AS*, **92**, 365–399, 1992.

Stone, E.C., C.M.S. Cohen, W.R. Cook, A.C. Cummings, B. Gauld, et al., The solar isotope spectrometer for the advanced composition explorer, *Space Sci. Rev.*, **86**, 357–408, 1998.

Torsti, J., E. Valtonen, M. Lumme, P. Peltonen, T. Eronen, et al., Energetic particle experiment ERNE, *Sol. Phys.*, **162**, 505–531, 1995.

Warmuth, A., and G. Mann, Kinematical evidence for physically different classes of large-scale coronal EUV waves, *A&A*, **532**, 151, 2011.

Vainio, R., L. Desorgher, D. Heynderickx, M. Storini, E. Flückiger, et al., Dynamics of the Earth's particle radiation environment, *Space Sci. Rev.*, **147**, 187–231, 2009.

Vedrenne, G., J.-P. Roques, V. Schönfelder, P. Mandrou, G.G. Lichti, et al., SPI: The spectrometer aboard INTEGRAL, *A&A*, **411**, L63–L70, 2003.